CHAPTER **7**

Phase Retrieval and Image Reconstruction for Astronomy

J. C. Dainty   *J. R. Fienup*

Blackett Laboratory   *Environmental Research*
Imperial College   *Institute of Michigan*
London SW7 2BZ, England   *Ann Arbor, Michigan 48107*

7.1 INTRODUCTION

In optical astronomy, the traditional way to obtain an object map or object intensity $f(x, y)$† is to use a single large telescope to record a conventional long-exposure image. This image can be enhanced, if necessary, by using the standard techniques of digital image processing. Although this may, at first sight, seem to be the most obvious method of estimating the object intensity, it suffers from two drawbacks. First, for earth-based observation, atmospheric turbulence limits the resolution obtainable to approximately 1 arc-sec (at the best observing sites), compared to the limit set by diffraction, $\alpha_{min} \sim \lambda/D$, where λ is the wavelength and D the telescope diameter. This limit is approximately 0.02 arc-sec for a 5-m telescope at a wavelength of 400 nm. Second, ignoring atmospheric turbulence, the diameter D of a single large telescope limits the resolution (as above) and it is difficult to imagine a telescope with a diameter greater than about 50 m in the foreseeable future.

The solution to the problem of limited resolution lies with a family of techniques which can be described as *interferometric imaging*. The basis of

† In astronomy, it is customary to use angular variables (α, β) instead of the spatial variables (x, y) used in this chapter.

231

these is the van Cittert–Zernike theorem [1, Sections 5.6 and 7.4], which, in the form of use in astronomy, states that the spatial coherence function $F(u, v)$ in the far field of a thermal light source is proportional to the Fourier transform of the object intensity $f(x, y)$. The spatial coherence of starlight can be measured by a variety of techniques, including speckle and Michelson interferometry.

Some of these interferometric methods are particularly suited to long-baseline and synthetic aperture techniques, in which the "diameter" D is potentially 1 km or more, providing the possibility of sub-milliarcsecond resolution in the future. Synthetic aperture techniques are, of course, widely used for imaging in radio astronomy.

Interferometric imaging techniques in optical astronomy all suffer from one major disadvantage: it is difficult, and sometimes impossible, to get an accurate estimate of the *phase* of $F(u, v)$. We are then faced with the problem of reconstructing the object intensity $f(x, y)$ either from $|F(u, v)|$ alone or with limited phase information. In both cases, the modulus (and phase information, if any) is known only within a finite region of the spatial frequency (u, v) plane, typically in a band extending from 0 to $\sqrt{u_{max}^2 + v_{max}^2} = D/(z\lambda)$, where z is the telescope focal length. In addition, $f(x, y)$ is known to be a nonnegative function and of finite extent.

In Section 7.2 we summarize the uniqueness aspects of phase retrieval from modulus-only data (this is discussed in Chapter 6 in more detail). Section 7.3 describes several algorithms for modulus-only data, for both special and general objects. Iterative algorithms have proved to be the most successful in practice, and Section 7.4 describes these and gives detailed instructions on how to obtain satisfactory reconstructions with a particular iterative approach. In the final section, we describe a number of solutions to the phase problem in optical astronomy that are specific to speckle and pupil plane (Michelson) interferometry. All of these utilize the (limited) phase information provided by these particular observing techniques.

Other reviews of stellar speckle interferometry can be found in [2–4].

7.2 UNIQUENESS OF PHASE RETRIEVAL FROM MODULUS DATA

In interferometric imaging, an attempt is made to measure the object's Fourier transform

$$F(u, v) = |F(u, v)| \exp[i\psi(u, v)]$$

$$= \int\int_{-\infty}^{\infty} f(x, y) \exp[-i2\pi(ux + vy)] \, dx \, dy, \qquad (7.2\text{-}1)$$

where $f(x, y)$ is the object's brightness or intensity distribution, $|F(u, v)|$ the Fourier modulus, and $\psi(u, v)$ the Fourier phase. In the extreme case of severe atmospheric turbulence, which is ordinarily the case at optical wavelengths, only $|F(u, v)|$ can be measured faithfully and all information about the phase, $\psi(u, v)$, is lost. Then two questions arise: first, how can one reconstruct $f(x, y)$, or equivalently reconstruct $\psi(u, v)$, from $|F(u, v)|$ given the *a priori* information that a physical brightness distribution is a real, nonnegative function? This first question is answered in Sections 7.3 and 7.4, which discuss various reconstruction algorithms. The second question is, given an image produced by a reconstruction algorithm, how does one know whether it is unique? That is, might not there be other real, nonnegative solutions having the same Fourier modulus?

First, it is necessary to recognize that $f(x, y)$, $f(x - x_0, y - y_0)$, and the image rotated by 180° (reflected through the origin), $f(-x - x_0, -y - y_0)$, all have the same Fourier modulus. This fundamental ambiguity does not cause much concern since it is the appearance of the object that is usually sought rather than its position. The position and the 180° rotational ambiguity can easily be resolved in many cases from a very low resolution image of the object. If the above fundamental ambiguities are the only ambiguities, we refer to the object as being unique; only ambiguous solutions having forms different from the object are considered ambiguous.

Until less than one decade ago, there was much pessimism that the phase retrieval problem could be solved or that the solution would be useful, because the available theory at the time, which was for one-dimensional functions, indicated that there were hopelessly many ambiguous solutions [5]. It can be shown that Fourier transforms of one-dimensional functions of finite support are analytic functions of exponential type. They are characterized by their complex zeros, i.e., the locations of the zeros of the (Fourier) function analytically extended into the complex plane, by

$$F(z) = \int_{-\infty}^{\infty} f(x) \, e^{-i2\pi zx} \, dx, \qquad (7.2\text{-}2)$$

where $z = u + iu'$, u being the physical real axis and u' the imaginary axis. If the set of complex zeros, for which $F(z) = 0$, are $\{z_n\}$, then the Fourier transform can be expressed as the Hadamard product

$$F(z) \propto \prod_{n=1}^{\infty} (1 - z/z_n). \qquad (7.2\text{-}3)$$

Given $|F(u)|^2 = F(u)F^*(u)$, the complex zeros of its analytic extension into the complex plane, $|F(z)|^2 = F(z)F^*(z^*)$, can be computed, but they include both the zeros $\{z_n\}$ of $F(z)$ and the zeros of $F^*(z^*)$, which are $\{z_n^*\}$.

If $F(z)$ has N complex zeros, then not knowing which of the $2N$ complex zeros of $|F(z)|^2$ go with $F(z)$ and which go with $F^*(z^*)$ leads to a 2^N-fold ambiguity. (Half of these solutions are the mirror images of the other half, reducing the ambiguity to 2^{N-1}-fold.) Ordinarily, N is comparable to the space–bandwidth product of $f(x)$, and so 2^N is an enormous ambiguity, making the one-dimensional problem seem hopeless. Only for the case of objects known to consist of two separated parts is the one-dimensional phase retrieval problem likely to be unique and therefore interesting [6–8].

The first indications that the situation is much different in two dimensions came from empirical reconstruction experiments [9,10]: images that were reconstructed looked like the simulated objects used to compute the Fourier modulus data. Those results gave hope that the two-dimensional problem may be soluble and unique, giving impetus to attempts to extend the one-dimensional theory of analytic functions to two dimensions in such a way that predictions concerning uniqueness could be made. Unfortunately, the theoretical level of understanding of the two-dimensional problem, while progressing [11–16], has not matched that available for the one-dimensional case.

If the object is approximated by an array of delta functions or by an array of numbers in a computer, then its Fourier transform reduces to a discrete Fourier transform which, with a change in variables, can be written as a polynomial of a complex variable. When this discrete approximation is made, one can understand the vast difference between the one-dimensional and two-dimensional phase retrieval problems [16]. It can be shown in the one-dimensional case that the zeros of the polynomial are analogous to the complex zeros for the continuous (analytic functions) case and that there are 2^{N-1} ambiguous solutions, where N is the number of factors into which the polynomial can be factored. Since the fundamental theorem of algebra states that a polynomial of degree N has N prime (irreducible) factors, one has a high degree of ambiguity for the one-dimensional case. As pointed out by Bruck and Sodin [16], it is known that polynomials of two complex variables are rarely factorable. Hence the two-dimensional phase retrieval problem is usually unique (ignoring noise issues). Chapter 6 describes the uniqueness issues for discrete functions in some detail.

Although most two-dimensional discrete objects are unique, one would like to know what conditions ensure uniqueness. As described in Section 6.3, objects whose Fourier transforms satisfy Eisenstein's criterion are unconditionally unique [17]. The type of support that the object must have (i.e., the set of points or the shape within which the object is nonzero) to satisfy this criterion is the only known support which guarantees unconditional uniqueness. The uniqueness of such objects can also be demonstrated by the existence of a recursive algorithm (a closed-form solution) that can

reconstruct such objects from their Fourier modulus via their autocorrelation functions [18]. This recursive algorithm can also be used to reconstruct in closed form objects having other supports as well, such as triangular supports having nonzero corners. But for these other objects the support must be known *a priori*, since there may be other solutions having different supports [18]. Objects that are unique among the class of objects having that given support include all objects for which the convex hull of their support is a polygon having no parallel sides [19,20]. Another such class of objects are those satisfying the holography condition: the object consists of an extended part plus a delta function (unresolved component) separated from the extended part by a distance greater than the diameter of the extended part. Then the extended part of the object is found as an isolated term in the autocorrelation function. Note, however, that objects satisfying the holography condition are not necessarily unique among all objects—they are only guaranteed to be unique among the class of objects satisfying the holography condition.

Although it remains to be proved definitively, the general feeling is that the physical case of interest, the two-dimensional continuous case, mirrors the discrete case and will, except for special objects, usually (but not always) be unique. It does not appear that the addition of small amounts of noise will change that assessment [21].

7.3 ALGORITHMS FOR PHASE RETRIEVAL FROM MODULUS

Since most phase retrieval/image reconstruction algorithms are performed on sampled data in the computer, we will employ the discrete Fourier transform

$$F(u, v) = |F(u, v)| \exp[i\psi(u, v)] = \mathscr{F}[f(x, y)]$$

$$= \sum_{x=0}^{N-1} \sum_{y=0}^{N-1} f(x, y) \exp[-i2\pi(ux + vy)/N] \qquad (7.3\text{-}1)$$

and its inverse

$$f(x, y) = N^{-2} \sum_{u=0}^{N-1} \sum_{v=0}^{N-1} F(u, v) \exp[i2\pi(ux + vy)/N], \qquad (7.3\text{-}2)$$

where u, v, x, and $y = 0, 1, 2, \ldots, N - 1$ (for simplicity, square arrays are assumed). Any computation of the discrete Fourier transform is, of course, accomplished by using the fast Fourier transform (FFT) method. Note that in order to compute $|F(u, v)|^2$ without aliasing it is required that $f(x, y)$ be zero outside $0 \leqslant x \leqslant M - 1$ and $0 \leqslant y \leqslant M - 1$, where $M \leqslant N/2$. The

autocorrelation of $f(x, y)$ is given by

$$r_f(x, y) = \sum_{x'=0}^{N-1} \sum_{y'=0}^{N-1} f(x', y')f(x' - x, y' - y) \qquad (7.3\text{-}3)$$

$$= \mathscr{F}^{-1}[|F(u, v)|^2]. \qquad (7.3\text{-}4)$$

The problem of reconstructing $\psi(u, v)$ or $f(x, y)$ from $|F(u, v)|$ or $r_f(x, y)$ has received much attention, especially within the past decade. Section 7.3.A describes several reconstruction methods that are tailored to special types of objects. Most of these methods work only for objects consisting of a collection of delta-function-like points or at least containing a pointlike component. Although they work only for such special cases, they are of interest because in astronomy the existence of pointlike stars is common and these methods tend to be simpler than the methods for more general objects. Section 7.3.B describes more general methods designed to work on most types of astronomical objects (objects of finite extent). Section 7.4 describes in more detail the iterative Fourier transform algorithm, which has been the most general and most successful reconstruction algorithm to date.

A. Algorithms for Special Types of Objects

1. Holography

The classic reconstruction method, discussed briefly in Section 7.2, is holography [22]: when the object includes a delta-function component (an unresolved point called the reference point) sufficiently separated from the rest of the object, then the object can be found as one term in the autocorrelation. Although holography was originally conceived for applications employing coherent light, the same principles apply for incoherent light if one has measured the modulus of the Fourier transform of the object [23,24].

2. Recursive Reconstruction Using Latent Reference Points

The closed-form recursive method [18] mentioned in Section 7.2 is akin to holography. It requires the existence of two or more reference points, making it more restrictive than the holography condition, but these reference points can be very close to the extended part of the object, making it less restrictive than the holography condition. These reference points satisfy the holography condition only for the far edge of the object, which is immediately reconstructed from the autocorrelation. After those edge points are

solved (including the reference points), then at least one of the autocorrelation values can be expressed as a sum of products of the previously solved points plus the product of an unknown point with a reference point. This single linear equation in a single unknown may be solved trivially. The rest of the points in the object are solved recursively in a similar manner. The reference points are referred to as latent since they cannot be used to solve for the interior points in the object until the exterior points are first reconstructed. This algorithm works only for particular types of sampled objects, including those for which the convex hull of their support is a polygon having no parallel sides† [20]. As mentioned in Section 7.2, one must know the support *a priori* to employ this algorithm. Except in special cases, given just the support of the autocorrelation one cannot find the support of the object [25]: one can only narrow down the possibilities.

3. *Difference Fourier Synthesis*

Some of the phase retrieval methods from x-ray crystallography [26] can be used for the astronomical application. One of these is difference Fourier synthesis [27]. Suppose the object consists of a collection of pointlike stars and one has an estimate of the object that contains some, but not all, of its stars. One creates a new image by (1) Fourier transforming the estimate of the object, (2) replacing the computed Fourier modulus by the true Fourier modulus while keeping the computed Fourier phase, and (3) inverse Fourier transforming the result. Under the assumptions mentioned above, it can be shown that the new image will contain the stars missing in the object's estimate, but at half their true value. So by taking the difference between the new image and the estimate of the object one can identify the locations and relative brightnesses of the missing stars and use that information to form a new estimate of the object. This algorithm must be applied iteratively because extraneous terms are produced in the new image along with the desired missing stars. This method was successful for pointlike objects but not for extended objects [27]. It is tantalizingly close to the iterative transform algorithm described in Section 7.4, which is applicable to a much more general class of objects.

4. *Products of Autocorrelations*

If the object consists of a collection of pointlike stars, then the autocorrelation $r_f(x, y)$ also consists of a number of pointlike terms. First one computes

---

† Note that Fig. 6(a) in [18] has two solutions rather than the single solution claimed. It would have a single solution if either point C′ or point C″ was zero.

the product $r_f(x - x_0, y - y_0)r_f(x, y)$, where the point (x_0, y_0) is one for which $r_f(x_0, y_0)$ is nonzero. Next one computes the triple product $r_f(x - x_1, y - y_1)r_f(x - x_0, y - y_0)r_f(x, y)$, where the point (x_1, y_1) is one for which $r_f(x_1 - x_0, y_1 - y_0)r_f(x_1, y_1)$ is nonzero. If the object points satisfy certain nonredundancy conditions, then the support of the triple product is identical to the support of the object (or the object rotated by 180°). Furthermore, the values of the object can be reconstructed in closed form by some very simple equations involving taking the cube root of (all but three of) the points in the triple product [25]. The nonredundancy conditions that the object must satisfy are that (1) the vector separations between three pairs of six distinct points must not sum to zero, (2) the vector separations between two different pairs of points must not be equal, and (3) the vector separation between one pair of points must not equal twice the vector separation between another pair of points. It is likely that a randomly distributed collection of stars would satisfy the nonredundancy conditions unless the number of stars in the image is large.

B. Methods Proposed for General Objects

The phase retrieval problem for general objects of finite support can be approached in a number of ways. Brute-force searching through all possible objects or all possible phases is, of course, impossible. For example, if there are K different values for each of the M^2 pixels of $f(x, y)$ that must be searched to see which objects agree with the given Fourier modulus, then the number of possibilities to be investigated is K^{M^2}, an overwhelming number, even for $K = 2$. If each of the particles in the universe were a computer that could search 10^9 objects per second, then it would take the age of the universe to search all possible binary objects for $M = 19$. Clearly, a very intelligent algorithm is needed to search through the possible objects to find one consistent with the Fourier modulus data.

Consider taking the modulus squared of both sides of Eq. (7.3-1) or simply use Eq. (7.3-3). In either case one has a system of N^2 nonlinear equations—one for each value of $|F(u, v)|^2$ or of $r_f(x, y)$—in M^2 unknowns, the values of $f(x, y)$ within its support. One could equally well treat the Fourier phases as the unknowns. Obviously, there is a high degree of redundancy in the set of equations since there are more equations than unknowns. Nevertheless, for large values of M and N the solution of a set of such nonlinear equations is a formidable task.

The classic approach to such a problem is to define an error metric for any given estimate for the object (or for the phase) and use a Newton–Raphson or a gradient search method to seek a solution, that is, an estimate

for which the error metric is zero. For example, the error metric could be

$$E_r = \sum_{x=0}^{N-1} \sum_{y=0}^{N-1} [r_g(x, y) - r_f(x, y)]^2, \qquad (7.3\text{-}5)$$

where $r_g(x, y)$ is the autocorrelation of $g(x, y)$, an estimate of $f(x, y)$. If $E_r = 0$ for a $g(x, y)$ that satisfies the object-domain constraints, then $g(x, y)$ is a solution. The solution is necessarily equal to $f(x, y)$ only if the phase retrieval problem is unique for $f(x, y)$, but at the reconstruction stage of the game this is not a problem since we are only concerned with finding a solution (or solutions).

The error metric E_r can be thought of as a function in an M^2-dimensional space where the values $g(x, y)$ are the coordinates of the space. The collection of the M^2 values of $g(x, y)$ can be thought of as an M^2-dimensional vector coordinate in that space. The problem is to find, within the subset of that space for which $g(x, y)$ satisfies the object-domain nonnegativity and support constraints, the point at which E_r is at a global minimum ($E_r = 0$ if no noise is present). One can seek the global minimum by starting with an estimate $g_0(x, y)$, computing the gradient of E_r at that point, and using that information to step down the side of the hill toward a lower value of E_r at a new estimate $g_1(x, y)$. Further steps are taken iteratively until the global solution is found or until stagnation occurs at a local minimum.

1. Newton-Raphson

The Newton–Raphson method [28] involves the local linearization of the problem by expressing $r_g(x, y)$ in Eq. (7.3-5) in a Taylor series expansion about the current estimate $g_k(x, y)$:

$$g(x, y) = g_k(x, y) + \Delta g(x, y), \qquad (7.3\text{-}6)$$

and keeping only up to first-order terms:

$$r_g(x, y) \simeq r_{g_k}(x, y) + \sum_{x'} \sum_{y'} \frac{\partial r_g(x, y)}{\partial g(x', y')} \Delta g(x', y'). \qquad (7.3\text{-}7)$$

Inserting this into the expression for E_r, E_r is minimized by setting equal to zero the partial derivatives of E_r with respect to $\Delta g(x_0, y_0)$ for each value of (x_0, y_0). This gives a system of M^2 linear equations in M^2 unknowns (the Δg's), which can be solved by inversion of an M^2 by M^2 matrix. A new estimate is given by Eq. (7.3-6) and the procedure is repeated. The matrix inversion takes on the order of M^6 operations, making this method computationally very intensive despite the fact that only a small number of iterations are required.

2. Gradient Search

Although requiring several times as many iterations as the Newton-Raphson method, gradient search algorithms are attractive because the amount of computation per iteration is far less. Ordinarily the computation of the gradient itself, if done with finite differences, would be very time-consuming, requiring one or two times M^2 FFTs. However, by a proper choice of the error metric it is possible to compute the entire gradient with only two FFTs [29]. If the error metric is defined in the Fourier domain by

$$E_F^2 = \sum_{u=0}^{N-1} \sum_{v=0}^{N-1} [|G(u, v)| - |F(u, v)|]^2, \qquad (7.3\text{-}8)$$

where $G(u, v)$ is the Fourier transform of the current estimate $g(x, y)$, then it can be shown that the bulk of the computation for the gradient can be accomplished by the first three steps of the iterative transform algorithm, which is described in Section 7.4.

In general, the kth iteration of a gradient search method would proceed by computing a desired direction, $d_k(x, y)$, in which to go from a given object estimate, $g_k(x, y)$, and take a step of size h_k in that direction:

$$g_k''(x, y) = g_k(x, y) + h_k d_k(x, y) \qquad (7.3\text{-}9)$$

For the steepest-descent gradient search method, $d_k(x, y)$ is just the negative of the partial derivative of E_F^2 with respect to $g(x, y)$. For the conjugate gradient method, $d_k(x, y)$ is a linear sum of the negative of the gradient and $d_{k-1}(x, y)$. After stepping to $g_k''(x, y)$ a test is made to see if it violates the object-domain constraints. It usually does, and a new estimate $g_{k+1}(x, y)$ is taken to be the function in object space satisfying the object-domain constraints that is closest to $g_k''(x, y)$. [In the language of Chapter 8, $g_k''(x, y)$ is projected onto the space of functions satisfying the constraints.] As for most applications, the steepest-descent method is very slow to converge, and the conjugate gradient method is much better [29]. Although the gradient search methods have not proved to converge as quickly as the algorithm described in Section 7.4, they have not yet been fully optimized and deserve further study.

3. Tracking of 1-D Complex Zeros

The method of tracking 1-D complex zeros [10] starts with one-dimensional radial cuts through the Fourier modulus. By the projection-slice theorem a radial cut through the 2-D Fourier transform is the 1-D Fourier transform of the projection of the object along a direction perpendicular to the direction of the radial cut. As mentioned in Section 7.2, there are 2^N

different solutions for a given 1-D radial cut, all of which can be computed by using different combinations of the conjugated or nonconjugated zeros $\{z_n, z_n^*\}$. Of these solutions only a small fraction will correspond to nonnegative projected images, and only these need be retained since the object brightness distribution is known to be nonnegative. As the angle of the cut is rotated slightly, the complex zeros should change in a continuous fashion, and so the complex zeros for one cut can be associated with the complex zeros for other cuts. By finding the complex zeros that yield nonnegative projected images over a range of cut angles, one can identify the set of zeros $\{z_n\}$ associated with each cut of the Fourier transform and solve the 1-D phase retrieval problem for each of the cuts, thereby solving the 2-D phase retrieval problem. This method has the disadvantage of having to compute 2^N different images for a number of cuts, which is computationally very burdensome. Application of this method gave one of the first indications that the 2-D problem is more likely to be unique than the 1-D problem [10].

4. Making 1-D Complex Zeros Consistent between Orthogonal Cuts

Employing a philosophy similar to that of the method described above, this method [30] computes the complex zeros of 1-D cuts through the 2-D Fourier modulus squared, and then from the complex zeros computes all 2^N different phase solutions for each cut. In this case the cuts are each line and each column of the 2-D Fourier transform. At each point in the Fourier domain a true solution must have a phase that is consistent with the phase of both orthogonal cuts. By checking consistency in phase at each point among all 2^N possible phases for each cut, it is possible to find what 2-D phase functions are consistent across the entire Fourier domain. A disadvantage of this method is the enormous computational burden of computing 2^N solutions for each of $2N$ cuts and comparing all the potential combinations.

5. Sampling Theorem Methods

The use of the sampling theorem is based on knowing that the object is of finite extent. If the object is zero outside a square of length L centered at the origin, then the Shannon sampling theorem gives

$$F(u, v) = \sum_p \sum_q F(p\,\Delta u, q\,\Delta v) \operatorname{sinc}\left(\frac{u - p\,\Delta u}{\Delta u}\right) \operatorname{sinc}\left(\frac{v - q\,\Delta v}{\Delta v}\right),$$

(7.3-10)

where $\Delta u = \Delta v = L^{-1}$. In the sampling theorem method [31,32], the samples $F(p\,\Delta u, q\,\Delta v)$ are estimated by $|F(p\,\Delta u, q\,\Delta v)|\exp[i\phi(p\,\Delta u, q\,\Delta v)]$, where

ϕ is an estimate of the unknown phase. This is inserted into the right-hand side of Eq. (7.3-10), which is evaluated at the half-integer coordinates, and the squared modulus is computed. Since adequate sampling of $|F(u, v)|^2$ is twice the sampling required for $F(u, v)$, and it is assumed that $|F(u, v)|^2$ was adequately sampled, the computed squared modulus values can be compared with the measured value of $|F(u, v)|^2$. This leads to a system of N^2 nonlinear equations in N^2 unknowns, which can be solved, for example, by the Newton-Raphson algorithm. This differs from the Newton-Raphson method described in Section 7.3.B.1—the set of nonlinear equations to be solved are different—but the computational complexity is the same.

A computationally more efficient version of the sampling theorem method has been devised [33]. Letting $v = 0$, Eq. (7.3-10) reduces to

$$F(u, 0) = \sum_p F(p\,\Delta u, 0)\,\text{sinc}\!\left(\frac{u - p\,\Delta u}{\Delta u}\right). \qquad (7.3\text{-}11)$$

Since the half-integer values of u along the $v = 0$ axis depend only on the sampled values along the $v = 0$ axis, the phase of $F(u, 0)$ can be determined by solving the one-dimensional problem, which involves only N nonlinear equations in N unknowns. In a similar fashion, given $F(p\,\Delta u, 0)$ for each integer value of p the phase of $F(p\,\Delta u, v)$ can be determined by solving a system of N nonlinear equations in N unknowns. The total required computation to solve $(N + 1)$ sets of N nonlinear equations in N unknowns, when solved by the Newton-Raphson method, involves $(N + 1)N^3$ operations times the number of iterations per 1-D solution, which is a great savings compared with the fully 2-D form described earlier. A disadvantage of this method is that each of the 1-D problems that is solved is just one of the 2^N ambiguous solutions that are always present for the 1-D problem. Consequently, this method will fail unless one starts with an initial estimate very close to the true solution or until one finds a way of incorporating more constraints in the algorithm.

A third variation on the sampling theorem method is the crude phase estimation method [34]. If one approximates the $\text{sinc}(u)$ kernels in Eq. (7.3-10) by a function that is unity at $u = 0$, a constant β at $u = \pm 1/2$, and zero for all other integer and half-integer values of u, then Eq. (7.3-10) simplifies to such an extent that the phase can be expressed in closed form as a function of the modulus of Eq. (7.3-10). The closed-form expression involves an arc cosine function which leads to twofold sign ambiguity, which can be resolved by a consistency check over a closed 2-D path in Fourier space [34]. While this method is computationally simple, it unfortunately yields only a very crude estimate of the Fourier phase owing to the crudeness with which the sinc function is approximated.

7.4 ITERATIVE TRANSFORM ALGORITHM

The iterative transform algorithm is a descendant of the Gerchberg-Saxton algorithm [35-37]. It bounces back and forth between the object domain, where *a priori* knowledge about the object—its nonnegativity and bounds on its support—is applied, and the Fourier domain, where the measured Fourier modulus data are applied. The iterative transform algorithm differs from the Gerchberg-Saxton algorithm both in the type of data and constraints available and in the more powerful object-domain operations applied for the hybrid input-output version of the algorithm. The iterative transform algorithm has been the most successful method for reconstructing nonnegative objects from the modulus of their Fourier transforms because it works for the most general types of objects, uses all the available data and constraints, is not highly sensitive to noise, and is not as computationally burdensome as most other methods. In Section 7.4.A the basic iterative algorithm is described. Additional details that will be helpful in the practical implementation of the algorithm are included in Section 7.4.B. In some difficult cases the basic iterative transform algorithm fails to converge to a solution. Distinct modes of stagnation have been identified and methods for overcoming them have been devised, as described in Section 7.4.C. Section 7.4.D shows an example of a simulation of noisy stellar speckle interferometry data, Fourier modulus estimation, and iterative transform reconstruction.

A. The Basic Iterative Algorithm

1. The Error-Reduction Algorithm

The simplest version of the iterative transform algorithm follows the philosophy of the Gerchberg-Saxton algorithm [35-37], and it is known as the error-reduction algorithm [9,29,38]. It can be viewed in a number of different ways: in terms of the method of successive approximations [39], as a form of steepest-descent gradient search [29], or as a projection onto sets in a Hilbert space (the Fourier modulus constraint being onto a nonconvex set, however, so convergence is not assured). The latter point of view is described in more detail in Chapter 8.

For the most general problem, the error-reduction algorithm consists of the following four steps (for the kth iteration): (1) Fourier transform $g_k(x, y)$, an estimate of $f(x, y)$, yielding $G_k(u, v)$; (2) make the minimum changes in $G_k(u, v)$ which allow it to satisfy the Fourier-domain constraints to form $G'_k(u, v)$, an estimate of $F(u, v)$; (3) inverse Fourier transform
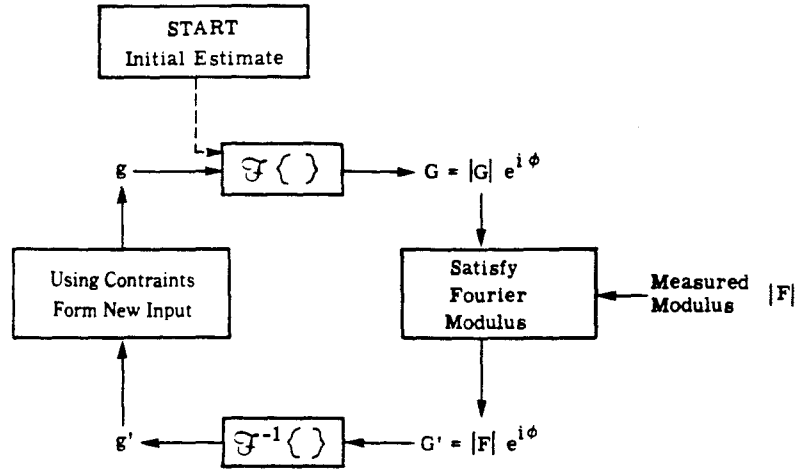
Fig. 7.4-1. Block diagram of the iterative transform algorithm.

$G'_k(u, v)$, yielding $g'_k(x, y)$, the corresponding image; and (4) make the minimum changes in $g'_k(x, y)$ that allow it to satisfy the object-domain constraints to form $g_{k+1}(x, y)$, a new estimate of the object. For phase retrieval for a nonnegative object from the Fourier modulus $|F(u, v)|$, these four steps are

Step 1: $G_k(u, v) = |G_k(u, v)| \exp[i\phi_k(u, v)] = \mathscr{F}[g_k(x, y)]$,   (7.4-1)

Step 2: $G'_k(u, v) = |F(u, v)| \exp[i\phi_k(u, v)]$,   (7.4-2)

Step 3: $g'_k(x, y) = \mathscr{F}^{-1}[G'_k(u, v)]$,   (7.4-3)

Step 4: $g_{k+1}(x, y) = \begin{cases} g'_k(x, y), & (x, y) \notin \gamma, \\ 0, & (x, y) \in \gamma, \end{cases}$ (7.4-4)

where γ is the set of points at which $g'_k(x, y)$ violates the object-domain constraints and where g_k, G'_k, and ϕ_k are estimates of f, F, and the phase ψ of F, respectively. The algorithm is typically started by using an array of random numbers for $g_0(x, y)$ or $\phi_0(u, v)$. Figure 7.4-1 shows a block diagram of the iterative transform algorithm.

For the astronomy problem, the object-domain constraints are the object's nonnegativity and a (usually loose) support constraint. Then the points in the set γ are those outside the assumed support and those within the support for which $g'_k(x, y) < 0$. The diameter of the object can be computed since it is just half the diameter of the autocorrelation; however, the exact support of the object in general cannot be determined uniquely from the support of the autocorrelation [25], and so the support constraint cannot be applied

tightly. For other problems, one may not have a nonnegativity constraint, but may have *a priori* knowledge of a tighter support constraint [40].

For the problem of phase retrieval from two intensity measurements [i.e., $|F(u, v)|^2$ and $|f(x, y)|^2$], $g'_k(x, y) = |g'_k(x, y)| \exp[i\theta'_k(x, y)]$ is complex-valued, and step 4 becomes

$$g_{k+1}(x, y) = |f(x, y)| \exp[i\theta_{k+1}(x, y)] = |f(x, y)| \exp[i\theta'_k(x, y)],$$

$$(7.4-5)$$

where $|f(x, y)|$ is the known modulus of the complex-valued object and θ_k is an estimate of the phase of the object. With this modulus constraint in the object domain, the error-reduction algorithm is precisely the Gerchberg–Saxton algorithm. In this chapter we consider only the problem of phase retrieval from a single intensity measurement, the squared Fourier modulus.

A measure of the convergence of the algorithm to a solution (a Fourier transform pair satisfying all the constraints in both domains) is the normalized root-mean-squared (NRMS) error metric in the Fourier domain,

$$E_F = \left[\frac{\sum_u \sum_v [|G(u, v)| - |F(u, v)|]^2}{\sum_u \sum_v |F(u, v)|^2} \right]^{1/2}, \tag{7.4-6}$$

or in the object domain,

$$E_o = \left[\frac{\sum\sum_{(x,y)\in\gamma} |g'_k(x, y)|^2}{\sum_x \sum_y |g'_k(x, y)|^2} \right]^{1/2}, \tag{7.4-7}$$

where γ is defined as in Eq. (7.4-4). Unless otherwise noted, the summations are performed over all points in image or Fourier space.

2. Proof of Convergence for the Error-Reduction Algorithm

It can be shown that the error-reduction algorithm "converges" in the weak sense that the squared error cannot increase with an increasing number of iterations [29]. This can be shown by considering an unnormalized squared error at the kth iteration,

$$e_{Fk}^2 = N^{-2} \sum_u \sum_v [|G_k(u, v)| - |F(u, v)|]^2 \tag{7.4-8}$$

$$= N^{-2} \sum_u \sum_v |G_k(u, v) - G'_k(u, v)|^2, \tag{7.4-9}$$

which by Parseval's theorem is

$$e_{Fk}^2 = \sum_x \sum_y |g_k(x, y) - g'_k(x, y)|^2. \tag{7.4-10}$$

Now compare this with the corresponding expression for the object-domain

error

$$e^2_{ok} = \sum_{(x,y)\in\gamma}\sum [g'_k(x, y)]^2 \qquad (7.4\text{-}11)$$

$$= \sum_x\sum_y |g_{k+1}(x, y) - g'_k(x, y)|^2. \qquad (7.4\text{-}12)$$

Both $g_k(x, y)$ and $g_{k+1}(x, y)$ by definition satisfy the object-domain constraints. Also, at any point (x, y), by definition $g_{k+1}(x, y)$ is the nearest value to $g'_k(x, y)$ that satisfies the object-domain constraints. Therefore for all points,

$$|g_{k+1}(x, y) - g'_k(x, y)| \leq |g_k(x, y) - g'_k(x, y)|, \qquad (7.4\text{-}13)$$

and therefore from Eqs. (7.4-10) and (7.4-12)

$$e^2_{ok} \leq e^2_{Fk}. \qquad (7.4\text{-}14)$$

Similarly, by Parseval's theorem

$$e^2_{ok} = N^{-2}\sum_u\sum_v |G_{k+1}(u, v) - G'_k(u, v)|^2. \qquad (7.4\text{-}15)$$

Since both $G'_k(u, v)$ and $G'_{k+1}(u, v)$ satisfy the Fourier-domain constraint, having modulus $|F(u, v)|$, and by definition $G'_{k+1}(u, v)$ is the nearest value to $G_{k+1}(u, v)$ that satisfies the Fourier-domain constraint, then

$$|G_{k+1}(u, v) - G'_{k+1}(u, v)| \leq |G_{k+1}(u, v) - G'_k(u, v)|. \qquad (7.4\text{-}16)$$

Therefore from Eqs. (7.4-9) and (7.4-15),

$$e^2_{F,k+1} \leq e^2_{ok}, \qquad (7.4\text{-}17)$$

and combining this with Eq. (7.4-14) gives the desired result

$$e^2_{F,k+1} \leq e^2_{ok} \leq e^2_{Fk}. \qquad (7.4\text{-}18)$$

That is, the error can only decrease, or at worst stay the same, at each successive iteration of the error-reduction algorithm.

3. The Hybrid Input–Output Algorithm

Although it works well for the problem of phase retrieval from two intensity measurements, the error-reduction algorithm usually converges very slowly for the problem of phase retrieval from a single intensity measurement being considered here [29]. Several modifications of the iterative transform algorithm were made and tested, and most of them converged faster than the error-reduction algorithm [29]. To date, the most successful version is the hybrid input–output algorithm, which replaces step

4 of the algorithm by [8,29]

$$g_{k+1}(x, y) = \begin{cases} g'_k(x, y) & (x, y) \notin \gamma \\ g_k(x, y) - \beta g'_k(x, y), & (x, y) \in \gamma, \end{cases} \quad (7.4\text{-}19)$$

where β is a constant feedback parameter. Values of β between 0.5 and 1.0 work well. When using the hybrid input-output algorithm, $g_k(x, y)$ is no longer an estimate of $f(x, y)$; it is instead the input function used to drive the output $g'_k(x, y)$ [which *is* an estimate of $f(x, y)$] to satisfy the constraints. Hence only the object-domain error E_o is meaningful. When using using the hybrid input-output algorithm, even E_o does not always correlate with image quality as well as one would like. For this reason one may prefer to perform a number of cycles of iterations, where one cycle consists of, say, 20-50 iterations of the hybrid input-output algorithm followed by 5-10 iterations of the error-reduction algorithm, and note E_o only at the end of a cycle.

For a more complete description of the various versions of the iterative algorithm, see [29]. Additional details concerning the implementation of the algorithm are given in Section 7.4B. A description of the algorithm as it applies to a number of different problems is given in [39].

B. Additional Aspects of the Iterative Transform Algorithm

In the past, some researchers have had varying success in applying the iterative transform algorithm to phase retrieval from a single intensity measurement. In this section, a number of additional aspects of making the iterative algorithm work are given as an aid to the practical implementation of the algorithm.

The information one must have available is an estimate $|\hat{F}(u, v)|$ of the modulus $|F(u, v)|$ of the Fourier transform of the object. Although the iterative transform reconstruction algorithm is not hypersensitive to noise, care must be taken to obtain the best possible estimate of the Fourier modulus, which may involve considerable compensation of the raw data [41], depending on how they are collected. In many circumstances one can estimate the expected value of the NRMS error of the data:

$$E_{|\hat{F}|} = \left[\frac{\sum_u \sum_v [|\hat{F}(u, v)| - |F(u, v)|]^2}{\sum_u \sum_v |F(u, v)|^2} \right]^{1/2}. \quad (7.4\text{-}20)$$

As described later, this is useful for deciding when one is close enough to a solution.

As the iterations progress, the NRMS error in the object domain, E_0, given by Eq. (7.4-7), should be computed. E_0 is a measure of how close

the current Fourier transform pair is to a solution. Note that the denominator of Eq. (7.4-7) is a constant that must be computed only once. When E_o goes significantly below $E_{|\hat{F}|}$ one has a solution consistent with the measured data and constraints to within the limits of the error in the given data. It is unlikely that E_o will ever go to zero because (1) diffraction by the telescope aperture causes side lobes in the image that extend beyond the support of the object and (2) noise in $|\hat{F}(u, v)|$ almost always results in a Fourier modulus that is inconsistent with either the nonnegativity constraint or any reasonable support constraint. Furthermore, in the presence of noise there will ordinarily exist an output image $g'(x, y)$ that is in better agreement with the noisy data than the true image is. Consequently, for the case of noisy data, a "solution" is not found until E_o is decreased to a level somewhat less than $E_{|\hat{F}|}$.

For the astronomy problem one has a nonnegativity constraint in the object domain. Furthermore, one can compute upper bounds on the support of the object in any of several ways [25]. The simplest way is to use a rectangle that is half the size, in each dimension, of the smallest rectangle that encloses the autocorrelation. If the actual support of the object is known *a priori*, it should, of course, be used. Any other types of *a priori* information should be used during the iterations if available. The support constraint can in general be defined by a binary mask which is unity within the support and zero outside; then the computations of Eqs. (7.4-4), (7.4-7), and (7.4-19) can be performed arithmetically without the use of logic, which is advantageous when using array processors.

There are many ways to pick an initial input to the algorithm. Although claims have been made that the crude phase estimation method described in Section 7.3.B.5 offers a superior starting point [34], others have found that random numbers do as well or better [42]. Having an initial input close to the true solution reduces the number of iterations required and might help to avoid some stagnation problems. If one of the reconstruction methods described in Section 7.5 has yielded an image, then that image would be an appropriate starting input. One can either view the other reconstruction method as a means for supplying starting inputs for the iterative transform algorithm or view the iterative transform algorithm as a means for "cleaning up" images reconstructed by the other method. If no other initial estimate for the object is available, one should use random numbers in the object domain or for the Fourier phase, giving an unbiased start to the algorithm. In the object domain, a convenient starting guess $g_o(x)$ can be formed by filling the support mask with random numbers. Another method [29] is to threshold the autocorrelation (at, say, 0.005 its maximum value), demagnify that by a factor of 2 in each dimension by discarding every other row and every other column, and finally fill the

resulting shape with random numbers. (Note that this shape does not necessarily contain the support of the object [25].)

The algorithm can be made to converge faster and avoid a stagnation problem (see Section 7.4.C.3) if the support mask is chosen to be somewhat smaller than the correct support for the first cycle or two of iterations. Since it is the incorrect support, the smaller support mask is inconsistent with the Fourier modulus and stagnation will eventually occur when it is used. Nevertheless, the smaller support mask helps to force most of the energy of the output, $g'(x, y)$, into a confined region in fewer iterations. After this has happened the support mask should be enlarged to the correct support constraint for the object. This enlargement of the mask could be done in more than one step if desired. When the algorithm has nearly finished reconstructing the object, it is often beneficial to make the support mask even larger than the correct support for the object. This helps to ensure that no parts of the object are being inadvertently truncated by the support constraint. The progression from a smaller support mask to a larger one also helps to avoid having edges of the output image biased toward falling right at the edges of the support mask.

Recall from Section 7.4.A that the heart of the algorithm consists of several cycles of iterations, where one cycle consists of K_1 iterations of the hybrid input–output algorithm [Eqs. (7.4-1)–(7.4-3) and (7.4-19)] followed by K_2 iterations of the error-reduction algorithm [Eqs. (7.4-1)–(7.4-4)]. Our experience has shown that values of K_1 from 20 to 100, of K_2 from 5 to 10, and of the feedback parameter β from 0.5 to 1.0 (use, say, 0.7) work well.

The discrete Fourier transforms are computed with the FFT algorithm. The sampling in the Fourier domain should be fine enough to ensure that the object domain array size is at least twice the width and height of the object itself, which is equivalent to achieving the Nyquist sampling rate for $|F(u, v)|^2$.

A straightforward method for evaluating Eq. (7.4-2) is to compute the phase from the real and imaginary parts of $G_k(u, v)$, then combine it with $|F(u, v)|$ to form $G'_k(u, v)$, and finally compute the real and imaginary parts of $G'_k(u, v)$ (which are required by the FFT) from its modulus and phase. Alternatively, one can employ

$$G'_k(u, v) = G_k(u, v)|F(u, v)|/[|G_k(u, v)| + \delta], \qquad (7.4\text{-}21)$$

where δ is a very small number used to prevent overflow problems in the rare event that $|G_k(u, v)| = 0$. (For some computers one can use $\delta = 0$ with no ill effects.)

If all goes well, the iterative transform algorithm will converge to a solution after a small number of cycles of iterations. If there are multiple solutions, the iterative transform algorithm is capable of finding any one

of them, depending on the starting input [43,44]. Confidence that the
solution is the one and only true solution can be increased by performing
two or more trials of the algorithm, each time using different random
numbers for the initial input.

In some cases the iterative transform algorithm will stagnate before
reaching a solution. The algorithm can be considered to have stagnated if
the error E_o is greater than $E_{|F|}$ and has failed to decrease after three
additional cycles. While some objects can be reconstructed very easily,
requiring only one or two cycles, other more difficult objects can require
many cycles comprising well over 1000 iterations. Consequently, one should
not too readily jump to the conclusion that the algorithm has stagnated. It
often occurs that very slow progress is made for many iterations, but then
the algorithm suddenly finds its way and rapid progress is made in just a
few iterations.

If the iterative transform algorithm does stagnate, then one can start over
with a different set of random numbers for the initial input; alternatively,
one can try other simple alterations of the algorithm. One can use a larger
value for β, say 1.2, causing larger changes to be made; but this should not
be carried out for too many iterations since it causes the algorithm to become
unstable. Use of a different support constraint mask may also be helpful.
For certain special modes of stagnation special methods have been devised
for overcoming the stagnation, as described below.

C. Methods for Overcoming Stagnation

Three particular modes of stagnation have been identified: those charac-
terized by (1) simultaneous twin images, (2) stripes, and (3) truncated
support. Methods have been devised to jump each of these hurdles. They
are briefly described in this section; further details can be found in [45].
(See Chapter 8 for another view of stagnation problems.)

1. Simultaneous Twin Images

Since both $f(x, y)$ and its twin image $f(-x, -y)$ have the same Fourier
modulus, the iterative transform algorithm is equally likely to reconstruct
either one. When the support of $f(x, y)$ is symmetric, the algorithm often
outputs a partially reconstructed image having features of both $f(x, y)$ and
$f(-x, -y)$ as illustrated in Fig. 7.4-2. In many cases the algorithm stagnates
with such an output image. (It is not a solution because $E_o > E_{|F|}$.) If the
algorithm has stagnated on an output image having a strong centrosymmetric
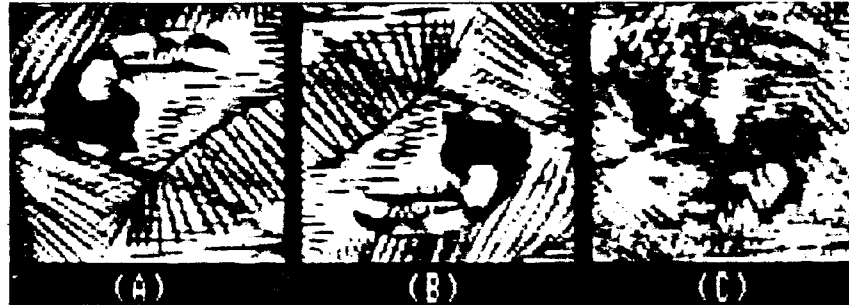component, then one would suspect this mode of stagnation. A method for

Fig. 7.4-2. Example of stagnation with simultaneous twin images. (A) Object $f(x, y)$; (B) twin image $f(-x, -y)$; (C) stagnated output image partially reconstructed from Fourier modulus, having features of both twins.

circumventing this stagnation problem is to use a reduced-area temporary support constraint for a few iterations. The temporary support should be highly asymmetric and should include one or two edges of the object's support but not the opposite edge. After a few iterations with the reduced-area support constraint, the symmetry in the output image may be sufficiently broken that on further iterations with the correct support constraint the iterative transform algorithm can converge to either $f(x, y)$ or its twin.

For example, to overcome the simultaneous twin images stagnation problem exhibited in Fig. 7.4-2C, a triangular support covering the lower right half of the true square support was used for 10 error reduction iterations. When further iterations of the algorithm were performed with the correct square support, it converged to the solution.

2. Stripes

The algorithm frequently stagnates in a mode in which the output image is a faithful representation of the object but with a pattern of stripes superimposed. This can be recognized by the fact that the stripes extend (although with less contrast) beyond the support of the object. The near-sinusoidal nature of the stripes is an indication that the phase errors occur in a symmetric pair of fairly well-defined areas in the Fourier domain. It has been observed that, if the iterative transform algorithm is applied more than once to the same Fourier modulus data but with different random initial inputs, then the stripes (if there are any) of each of the reconstructed images tend to have different frequencies and orientations [46], which means that the errors occur in different areas of the Fourier domain. Figures 7.4-3A to 7.4-3D show an example of this.
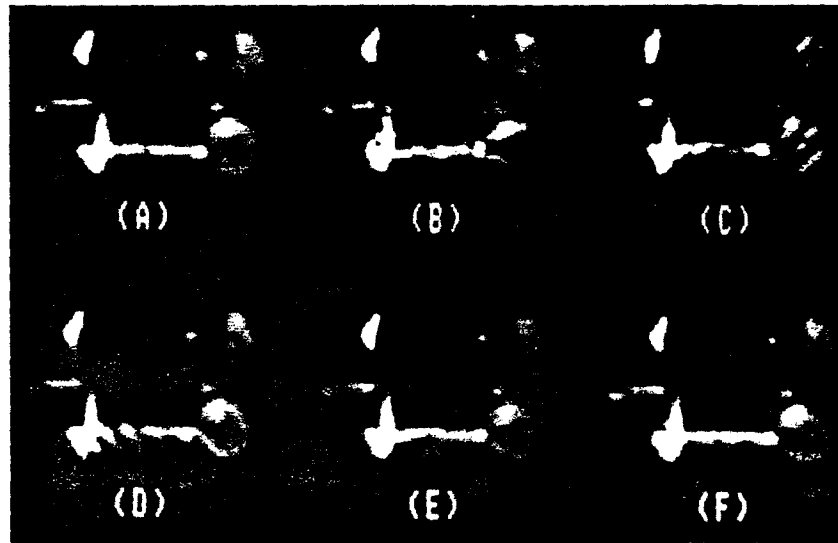
Fig. 7.4-3. Example of stagnation with stripes and overcoming it by the voting method. (A) Object; (B–D) images partially reconstructed by the iterative transform algorithm, each from a different random starting input and each having a different set of stripes superimposed on an otherwise good-quality image; (E) output of the voting method; (F) output image after further iterations.

One method for solving this stagnation problem is the voting method [45]. The iterative transform algorithm is applied three times, each time with a different random initial input to produce three different striped images, as shown in Figs. 7.4-3B to 7.4-3D. (If one of them has no stripes, then, of course, the problem is solved.) By cross-correlations the relative translations and orientations of the three images are determined and corrected so that they are made to be in perfect registration. The Fourier transforms of the three images are compared. At each point the two complex Fourier values that are closest are averaged and the third (assumed to have a phase error) is discarded. The resulting composite Fourier function is inverse transformed to produce the corresponding output image. Then further iterations of the iterative transform algorithm are performed. For example, Fig. 7.4-3E shows the output of the voting method applied to the images shown in Figs. 7.4-3B to 7.4-3D, and Fig. 7.4-3F shows the result of further iterations.

A second method for overcoming stagnation with stripes is the patching method [45]. It requires that only two striped images be produced and made to be in registration. For each of these images the area of the support

of the object is zeroed out, leaving just the stripes in the area outside the object's support. These stripes are Fourier transformed, and the resulting Fourier modulus arrays are used to determine what areas in the Fourier domains have phase errors associated with the stripes. It is assumed that those areas are different for each of two striped images. A new composite Fourier transform is set equal to the Fourier transform of the first striped image where it is not affected by the phase errors and to the Fourier transform of the second striped image where the first is affected by the phase errors. Both methods of overcoming the problem of stagnation with striped images have been shown to be effective [45].

3. Truncated Support

Since $f(x - x_0, y - y_0)$ has the same Fourier modulus as $f(x, y)$, the location of the object's support is arbitrary. Frequently the image partially reconstructed by the algorithm is not in perfect registration with the support constraint. Then enforcing the support constraint causes an inadvertent truncation of part of the desired image, causing the algorithm to stagnate. In addition to the enlarging support method described in Section 7.4.B, a method of combating this stagnation problem is to dynamically translate either the support constraint or the image.

The amount of translation to be used can be determined as follows. Compute the total energy of the output image $g'_k(x, y)$ (i.e., square and sum) over the area of the support constraint for the current position of the support constraint and for the support constraint translated by one or two pixels in every direction. The support constraint should be translated to the position for which the energy is maximized. Alternatively, compute the cross-correlation of $g'_k(x, y)$ with the support mask, and translate according to the peak of the cross-correlation. This can be done occasionally or at every iteration. This method would be particularly effective if, just prior to performing it, a support constraint larger than the usual support were used for a few iterations; that would give the truncated part of the image a chance to establish itself.

D. Iterative Reconstruction Example

In this section, the results of a computer experiment in which stellar speckle interferometry [47] was realistically simulated—including the effects of atmospheric turbulence and photon noise—and reconstruction from noisy Fourier modulus data by the iterative transform algorithm are shown [46]. (See Section 7.5.A for a description of stellar speckle interferometry.)
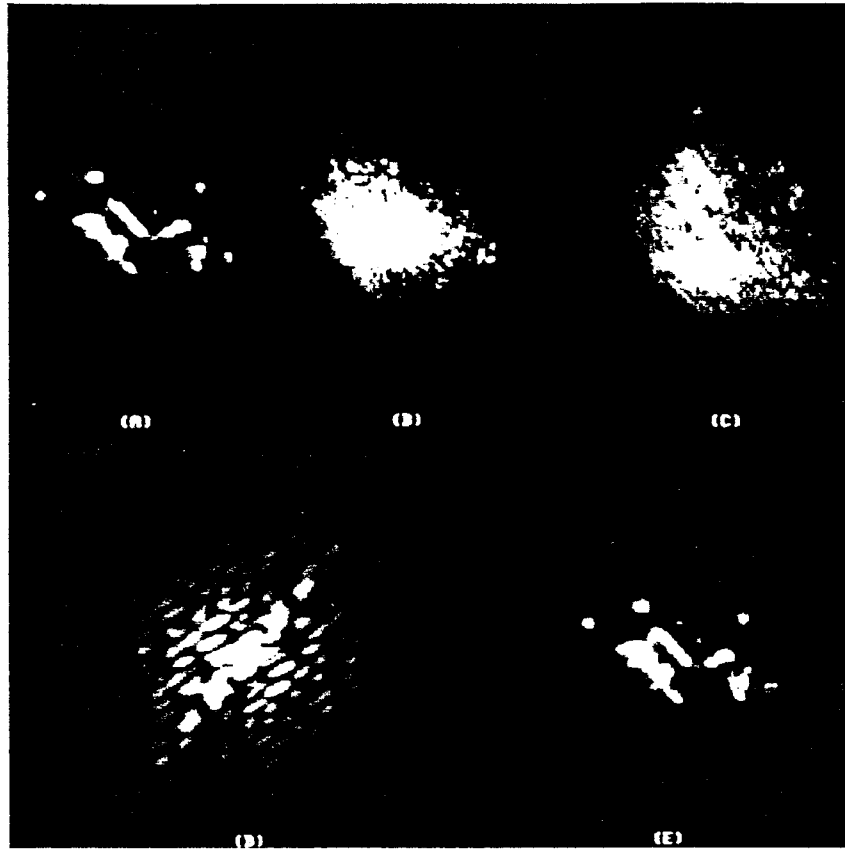
Fig. 7.4-4. Image reconstruction example. (A) Undegraded object; (B, C) examples of degraded images simulated to include the effects of atmospheric turbulence and photon noise; (D) Fourier modulus estimate computed from the degraded images; (E) image reconstructed by using the iterative transform algorithm.

An undegraded object, a low-pass filtered, digitized photograph of a satellite, shown in Fig. 7.4-4A, was convolved with 156 different point spread functions to produce 156 different blurred images. Each of the point spread functions represented a different realization of the effects of the turbulent atmosphere. The blurred images were then subjected to a Poisson noise process to simulate the effects of photon noise. For this example, there were approximately 300,000 photons per degraded image (or on the order of 100 photons per pixel over the extent of the object), which is realistic for objects of this type when imaged through a telescope of diameter 1.6 m. Two of the resulting 156 degraded images are shown in Figs. 7.4-4B and 7.4-C. The degraded images were then processed by Labeyrie's [47] method as modified

by Goodman and Belsher [48]. The estimate of the modulus of the Fourier transform of the object is given by [46]

$$F(u, v) = W(u, v)\left[\frac{\sum_{m=1}^{M}|I_m(u, v)|^2 - N_p}{\sum_{m=M+1}^{2M}|T_m(u, v)|^2}\right]^{1/2}, \qquad (7.4\text{-}22)$$

where $I_m(u, v)$ is the Fourier transform of the mth degraded image, N_p is the total number of photons detected (it is subtracted in order to compensate for a noise bias term that arises in the power spectrum due to photon noise [48]), $T_m(u, v)$ is the Fourier transform of the mth point-spread function [to provide compensation for the modulation transfer function (MTF) of the speckle interferometry process], and the weighting factor $W(u, v)$ is the MTF due to the telescope aperture. In practice, the denominator of this expression would be obtained by making measurements on a reference star through an atmosphere having the same statistics as that which blurred the images or by using a model of the effects of atmospheric turbulence. The term $W(u, v)$ was included in order to restore the natural MTF due to the telescope aperture, which was removed by the denominator of Eq. (7.4-22). Figure 7.4-4D shows the resulting Fourier modulus estimate.

The object was reconstructed (or, equivalently, the Fourier phase was retrieved) using the hybrid input–output algorithm alternately with the error-reduction algorithm. The result, shown in Fig. 7.4-E, agrees very well with the original object shown in Fig. 7.4-4A, despite the noise present in the Fourier modulus data. Good reconstructed images were also obtained when only one-tenth as many photons were assumed to be available [46].

For this reconstruction example, Fig. 7.4-5 shows E_o versus the number of iterations and Fig. 7.4-6 shows the output image at various stages. The
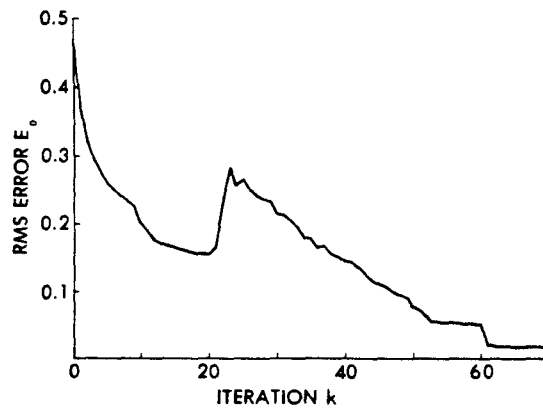

Fig. 7.4-5 Normalized root-mean-squared (NRMS) error metric, E_o, versus iteration number for the example.
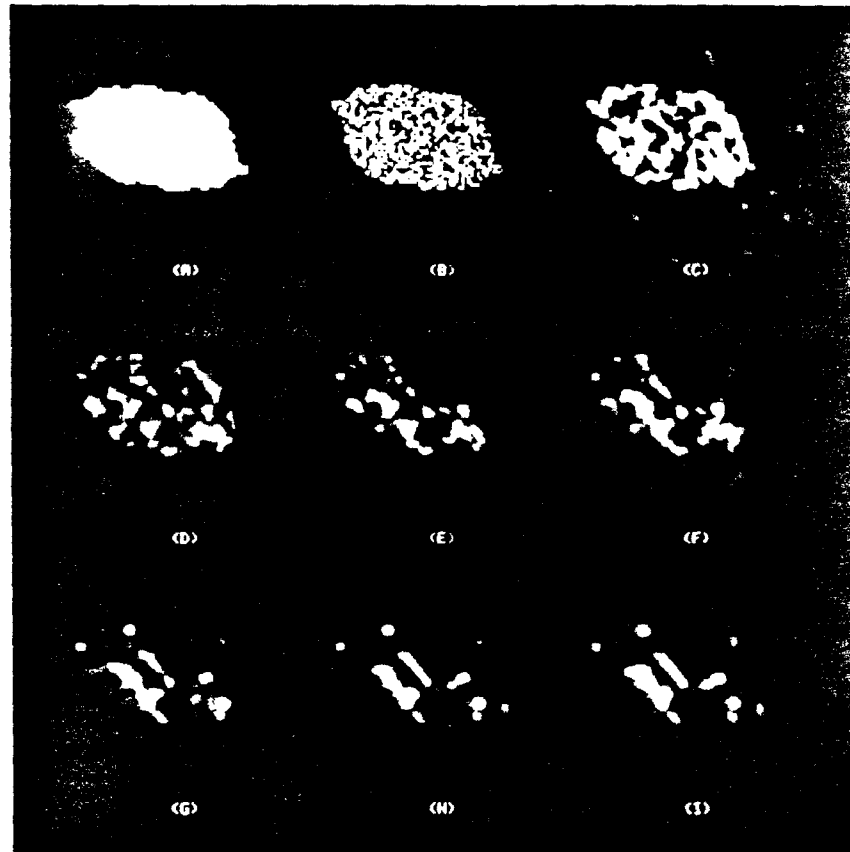
Fig. 7.4-6. Details of the image reconstruction example. (A) Mask array defining the support constraint for the first 10 iterations; (B) initial input to the iterative transform algorithm; (C-I) output images—number of iterations: (C) 1, (D) 5, (E) 20, (F) 25, (G) 35, (H) 45, (I) 55.

starting input used, shown in Fig. 7.4-6B, was the randomized, demagnified autocorrelation described in Section 7.4.B, using a threshold value of 0.0004 times the peak of the autocorrelation. For the first 10 iterations, the error-reduction algorithm was used and the mask defining the support constraint was chosen to be the region over which the autocorrelation function, spatially demagnified by a factor of 2, exceeded 0.0004 of its maximum value, providing a fairly tight diameter constraint (it is just the support of Fig. 7.4-6B, which is shown in Fig. 7.4-6A). For iterations 11 to 20 the error-reduction algorithm was used, and the mask for these and the remaining iterations was chosen to be a square of length 64 pixels, which is larger

than the actual object extent of about 60×40 pixels (embedded in an array of 128×128 pixels). The error E_o decreased rapidly at first, and the visual appearance of the output image improved substantially from the first iteration, shown in Fig. 7.4-6C, to the fifth iteration, shown in Fig. 7.4-6D. The error decreased suddenly at the tenth iteration since some positive-valued points that were inside the second mask but outside the first mask were no longer counted as contributing to E_o. By the twentieth iteration the error-reduction algorithm was converging very slowly, and the output image, shown in Fig. 7.4-6E, is only slightly improved over that in Fig. 7.4-6D. For interations 21 to 60 the hybrid input–output algorithm, with $\beta = 1$, was used. At first E_o increased sharply, although, as shown in Fig. 7.4-6F, the output image at iteration 25 appeared no worse than at iteration 20; then E_o decreased fairly rapidly until stagnation at $E_o \simeq 0.05$ at about iteration 55. Output images at iterations 35, 45, and 55 are shown in Figs. 7.4-6G, H, and I, respectively. For iterations 61 to 70 the error-reduction algorithm was used, for which E_o dropped suddenly from 0.05 to 0.02, although the visual appearance of the reconstructed image remained the same as for iteration 55.

This final value of E_o is somewhat less than 0.03, the normalized rms error of the Fourier modulus estimate itself.

Reconstruction experiments do not always proceed as smoothly as the one described above. When stagnation occurs, the methods described in Sections 7.4.B and 7.4.C should be employed.

7.5 SOLUTIONS SPECIFIC TO MEASUREMENT TECHNIQUES

We have assumed so far in this chapter that only the modulus of the Fourier transform $|F(u, v)|$ of the object intensity $f(x, y)$ is known and have combined these data with the *a priori* knowledge that the object is nonnegative and of finite extent to achieve a reconstruction of the object. Astronomical observing techniques based on either speckle (image plane) or Michelson (pupil plane) interferometry can yield data in addition to the modulus of the Fourier transform: for example, speckle interferometry gives, in addition to a diffraction-limited estimate of the modulus, a low-resolution image of the object, i.e., an estimate of both the modulus and phase of the transform at low spatial frequencies. These additional data may in some cases be sufficient to determine the object intensity without any ambiguity. Since the different methods are specific to the observing technique, they are described separately under the headings of speckle interferometry and Michelson interferometry.

A. Object Recovery from Speckle Interferometry Data

1. Basic Speckle Technique

Speckle interferometry was invented by A. Labeyrie [47] in 1970 as a means of obtaining *diffraction-limited* resolution (but not images) from large telescopes, despite the presence of atmospheric turbulence or "seeing." The method is illustrated in Fig. 7.5-1 for an unresolved star, binary stars of two separations, and a resolved star. A large number of short-exposure (~10 ms) photographs are taken, each through a different realization of the atmosphere, typical examples being shown in row B (see also Fig. 7.5-2). For a binary star, each component produces an identical speckle pattern and a "double-speckle" effect may be visible in each short-exposure image in favorable circumstances. The optical diffraction pattern, or squared modulus of the Fourier transform, of each photograph is shown in row C—the signal-to-noise ratio is low for a single record and may be improved by adding many such diffraction patterns (row D). The unresolved object has a diffraction halo of relatively large spatial extent, the binaries give fringes of period inversely proportional to their separation, and the resolved object gives a diffraction halo whose diameter is inversely proportional to the diameter of the object. By taking a further Fourier transform of each ensemble-averaged diffraction pattern, we obtain the average spatial autocorrelation of the diffraction-limited images of each object (row E).

In mathematical terms, one estimates either the average spatial autocorrelation $\langle g(x, y) \star g(x, y) \rangle$ or the power† spectrum $\langle |G(u, v)|^2 \rangle$ of the image intensity $g(x, y)$, where $\langle \ \rangle$ denotes the ensemble average, from a finite number of frames. It can be shown that the image power spectrum is related to that of the object, $|F(u, v)|^2$, through the speckle transfer function $\langle |T(u, v)|^2 \rangle$:

$$\langle |G(u, v)|^2 \rangle = |F(u, v)|^2 \langle |T(u, v)|^2 \rangle, \qquad (7.5\text{-}1)$$

where

$$\langle |T(u, v)|^2 \rangle = |\langle T(u, v) \rangle|^2 + T_D(u, v)/N_s, \qquad (7.5\text{-}2)$$

and all spatial frequencies are referred to those of the image (formed by a telescope of focal length z using light of wavelength λ). In Eq. (7.5-2), $\langle T(u, v) \rangle$ is the average (seeing-limited) transfer function, $T_D(u, v)$ is the *diffraction-limited* transfer function of the telescope, and N_s is the average number of speckles per frame [$\approx 2.3(D/r_0)^2$], where r_0 is the atmospheric seeing parameter.

---

† Strictly speaking, this should be called the average *energy* spectrum [3, p. 260].
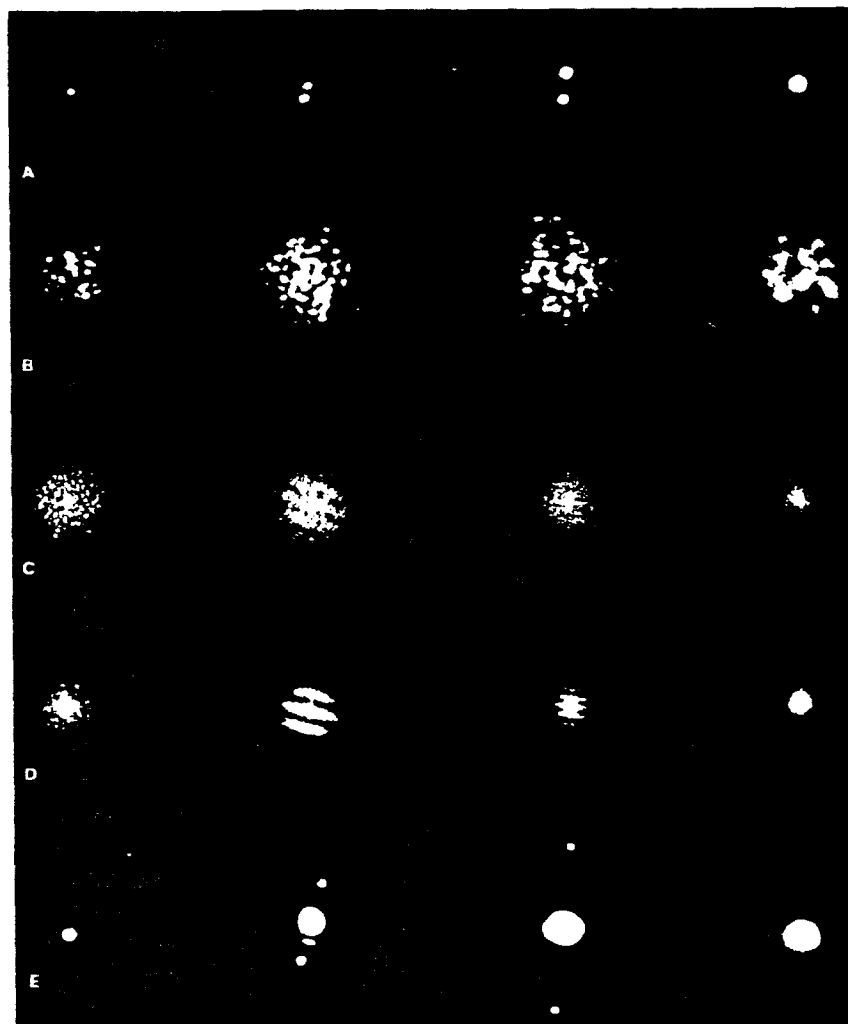
Fig. 7.5-1. Laboratory simulation showing the principles of stellar speckle interferometry. (A) Objects; (B) typical short-exposure photographs; (C) diffraction patterns of row B; (D) sum of 20 diffraction patterns; (E) diffraction patterns of row D (not at the same scale as row A). (Courtesy of A. Labeyrie, CERGA.)

The key feature of speckle interferometry is that the speckle transfer function $\langle |T(u, v)|^2 \rangle$ is nonzero up to the diffraction limit of the telescope, as given by Eq. (7.5-2), allowing the object power spectrum $|F(u, v)|^2$, or equivalently the object autocorrelation $f(x, y) \star f(x, y)$, to be estimated up to the diffraction limit of the telescope. Note that the basic technique does
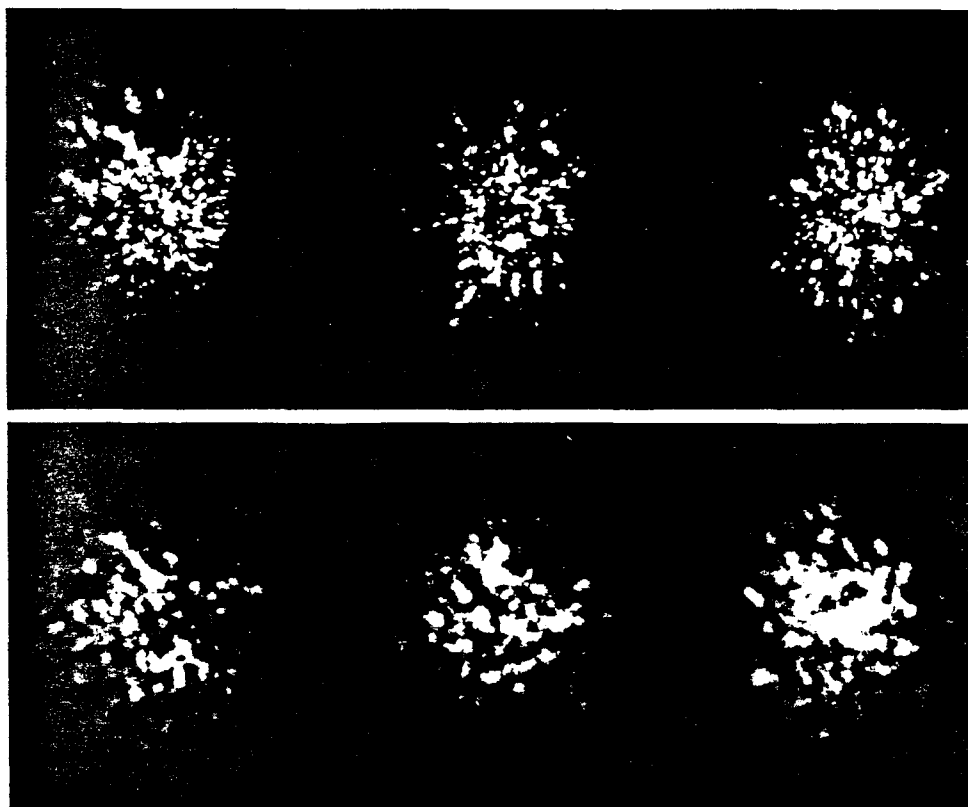
Fig. 7.5-2. Short-exposure photographs of an unresolved point source.(upper row) and a resolved star, α-Orionis (lower row), taken on a 4-m telescope. The exposure time and filter bandwidth are 10^{-2} s and 10 nm, respectively. (Courtesy of B. L. Morgan and R. J. Scaddan, Imperial College, London.)

not give the object intensity itself: to address this problem, one must use one of the phase retrieval algorithms described earlier or one of the speckle *imaging* techniques described below.

2. Shift-and-Add Method

The first speckle imaging technique to be suggested used the notion that the individual speckles in a short-exposure image resemble diffraction-limited images of the object. Figure 7.5-2 compares short-exposure images of a point source and a resolvable star, and there is a clear qualitative difference between the speckle structure in the two cases. By averaging the

centroided versions of selected bright speckles, Lynds *et al.* [49] were able to reconstruct a map of the red giant α-Orionis. The procedure was made a little more systematic and generalized by Bates and Cady [50], who suggested that the brightest speckles in the image be *shifted* to the origin and the entire images *added* (hence "shift-and-add").

There are two problems with this method that make it unlikely to be of practical significance for most objects. First, to be able to implement the method it is necessary to identify individual speckles, and this can be done only if there are more than approximately 10^5 detected photons per frame, implying an object brighter than about 5th magnitude in the visible. Second, each speckle is obviously *not* an image of the object and there is no linear transfer function for this technique, making it difficult to reconstruct reliable quantitative object maps. The Bates and Cady extension can give good results if the image contains a very bright unresolved component [51].

3. Cross-Power Spectrum Method

This method, first suggested by Knox and Thompson [52], makes use of the fact the *phase difference* between two values of $F(u, v)$, separated by $(\Delta u, \Delta v) < r_0/\lambda z$ in spatial frequency, is present in the original speckle data $g(x, y)$ and can be extracted by computing the cross-power spectrum $\langle G(u, v)G^*(u + \Delta u, v + \Delta v)\rangle$. A straightforward analysis shows that

$$\text{phase}\{\langle G(u, v)G^*(u + \Delta u, v + \Delta v)\rangle\}$$
$$= \text{phase}\{F(u, v)\} - \text{phase}\{F(u + \Delta u, v + \Delta v)\}$$
$$+ \text{phase}\{\langle T(u, v)T^*(u + \Delta u, v + \Delta v)\rangle\}. \qquad (7.5\text{-}3)$$

The phase of a complex quantity has meaning only if its modulus is nonzero, so that from Eq. (7.5-3) there are two conditions to be met if phase differences of $F(u, v)$ are to be computed from the phase of the cross-spectrum:

(i) $|\langle T(u, v)T^*(u + \Delta u, v + \Delta v)\rangle| \neq 0$,
(ii) $\text{phase}\{\langle T(u, v)T^*(u + \Delta u, v + \Delta v)\rangle\}$ either known or zero.

If we assume that the complex amplitude in the telescope pupil has complex Gaussian statistics and that its autocorrelation function has a Gaussian shape, i.e., the "seeing" transfer function $T_s(u, v)$ is Gaussian, then it can be shown [3, p. 303] that

$$\langle T(u, v)T^*(u + \Delta u, v + \Delta v)\rangle \simeq \langle |T(u, v)|^2\rangle|T_s(\Delta u/2, \Delta v/2)|^2. \quad (7.5\text{-}4)$$

That is, the Knox–Thompson transfer function is simply the product of the normal speckle transfer function [Eq. (7.5-2)] at (u, v) and the squared

modulus of the seeing transfer function at $(\Delta u/2, \Delta v/2)$. It follows that the modulus of the Knox–Thompson transfer function is nonzero up to the diffraction limit of the telescope provided that $\Delta u/2$ and $\Delta v/2$ are less than $(r_0/\lambda z)$, the width of the seeing transfer function. It also follows that

$$\text{phase}\{\langle T(u, v) T^*(u + \Delta u, v + \Delta v)\rangle\} \simeq 0.$$

The problem of finding the phase of $F(u, v)$ given the phase differences for frequencies separated by $(\Delta u, \Delta v)$ is identical to that of finding a wave front from sheared interferograms [53]. Simple "bootstrapping" of the phase differences, starting at the origin of the spatial frequency plane, leads to cumulative errors at higher frequencies and in two dimensions yields phase values at a given frequency that depend on the path taken in the frequency plane: averaging these values is not the best way to deal with this problem. A least-squares solution is straightforward to implement, using an iterative technique to solve the usual matrix equation (the matrix that relates the phase differences to the phase values is sparse) [54].

The assumptions leading to Eq. (7.5-4) are not particularly realistic and it remains to be seen how sensitive this technique is to the atmospheric statistics.

4. Triple Correlation Method

The average triple correlation $\langle g^{(3)}(\mathbf{x}_1, \mathbf{x}_2)\rangle$ of the image intensity $g(\mathbf{x})$, or equivalently its Fourier transform, the bispectrum $\langle G^{(3)}(\mathbf{u}_1, \mathbf{u}_2)\rangle$, contains information on the phase of $G(\mathbf{u})$ and hence on the phase of the object transform [55,56]. Here we use the notation $\mathbf{x} = (x, y)$ and $\mathbf{u} = (u, v)$. The triple correlation and bispectrum are, for a real function $g(\mathbf{x})$, defined by

$$g^{(3)}(\mathbf{x}_1, \mathbf{x}_2) = \int\limits_{-\infty}^{\infty}\!\!\int g(\mathbf{x})g(\mathbf{x}+\mathbf{x}_1)g(\mathbf{x}+\mathbf{x}_2)\, d\mathbf{x} \qquad (7.5\text{-}5)$$

and

$$G^{(3)}(\mathbf{u}_1, \mathbf{u}_2) = G(\mathbf{u}_1)G(\mathbf{u}_2)G(-\mathbf{u}_1 - \mathbf{u}_2). \qquad (7.5\text{-}6)$$

The average bispectrum of the image is related to that of the object through a bispectrum transfer function $\langle T^{(3)}(\mathbf{u}_1, \mathbf{u}_2)\rangle$,

$$\langle G^{(3)}(\mathbf{u}_1, \mathbf{u}_2)\rangle = F^{(3)}(\mathbf{u}_1, \mathbf{u}_2)\langle T^{(3)}(\mathbf{u}_1, \mathbf{u}_2)\rangle. \qquad (7.5\text{-}7)$$

If it is assumed that complex amplitude in the telescope pupil has Gaussian statistics, then it can be shown [55] that the bispectrum transfer function is real and nonzero over the diffraction-limited portion of the

(u_1, u_2) volume: it follows that the phase of the image bispectrum equals that of the object bispectrum.

To see how the phase of the object spectrum (which is Hermitian) can be calculated recursively from that of the object bispectrum, consider a one-dimensional sampled bispectrum $F_{l,m}^{(3)}$:

$$F_{l,m}^{(3)} = F_l F_m F_{-l-m}.\qquad(7.5\text{-}8)$$

Denoting the phase of the object spectrum by ψ_n and that of the bispectrum by $\beta_{l,m}$, the phase factors satisfy the equation

$$\exp[i\psi_n] = \exp[i(\psi_m + \psi_{n-m} - \beta_{n-m,m})],\qquad(7.5\text{-}9)$$

where the substitution $n = l + m$ has been made. Note that both ψ_0 and ψ_1 may be set equal to zero as the object is real and its absolute position is not of interest.

Now consider Eq. (7.5-9) with $m = 1$ and $n = 2, 3, 4, \ldots$:

$$\exp[i\psi_n] = \exp[i(\psi_1 + \psi_{n-1} - \beta_{n-1,1})],\qquad(\psi_1 = 0).\qquad(7.5\text{-}10)$$

Clearly, $\psi_2, \psi_3, \ldots$ can be found by simple recursion with $n = 2, 3, \ldots$. In fact, the process can be repeated for different values of m to yield a more accurate estimate of the phase at each spatial frequency. The method is in some ways similar to, but more general than, the cross-power spectrum technique described in Section 7.5.A.3.

The triple correlation method is illustrated in Fig. 7.5-3 for a one-dimensional projection of the double star ω-Leonis. For the more interesting case of two-dimensional objects, the reconstruction of the object spectrum from the bispectrum is computationally quite reasonable—the problem lies in computing the average bispectrum, which is a four-dimensional function. Nevertheless, the triple correlation method appears to be the most promising technique of speckle imaging at the present time.

5. Exponential Filter Method

For discrete objects, the object spectrum can be written as a polynomial or z-transform, as discussed in Section 6.1. For modulus-only reconstruction in one dimension, the possibility of ambiguities arises because the zeros of the power spectrum of the object include both the zeros of the original object and their inverses: in the one-dimensional case it is not in general possible to distinguish the correct zeros from their inverses, given only the Fourier modulus. The cross-spectrum method eliminates this ambiguity by rotating the "inverse" zeros by a known amount [57], thus enabling them to be distinguished from the correct ones even in the one-dimensional case. The triple correlation method also allows the zeros of the object spectrum
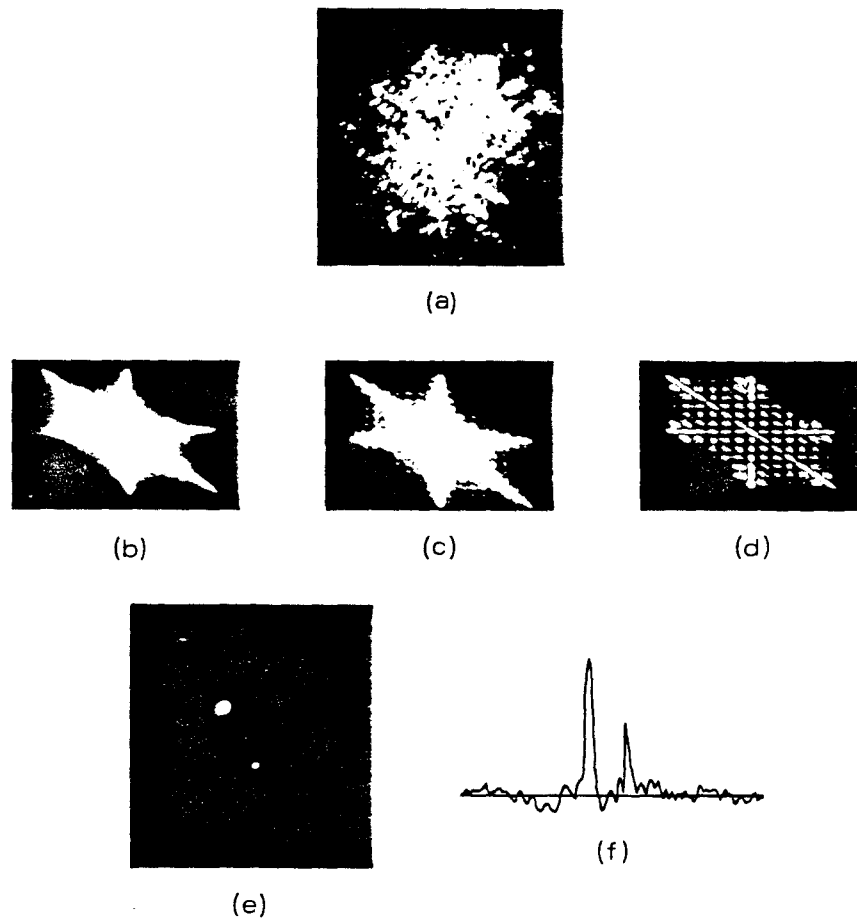
(a)

(b)

(c)

(d)

(e)

(f)

Fig. 7.5-3. Illustration of the triple correlation method in one dimension on the double star ω-Leonis. (a) Typical short-exposure speckle photograph; (b) bispectrum transfer function; (c) average bispectrum of speckle image calculated from 300 exposures; (d) object bispectrum found from (b) and (c); (e) reconstructed image; (f) scan through reconstructed image. (Courtesy of A. W. Lohmann and G. Weigelt, University of Erlangen.)

to be identified correctly from the zeros of the triple correlation [56]. The exponential filter method provides a third way of distinguishing the correct zeros from their inverses: in this case the correct zeros are moved out radially in the complex plane by a known amount.

In this method, one records the instantaneous image intensity $g(x, y)$ in the usual way and computes the average power spectrum $\langle |G(u, v)|^2 \rangle$. A

second power spectrum, $\langle |G'(u, v)|^2 \rangle$ of $g(x, y)p(x, y)$, where $p(x, y)$ is a special modifying function, is also computed. Walker [58] showed that if the modifying function has the property

$$p(x_1 + x_2, y_1 + y_2) = p(x_1, y_1)p(x_2, y_2),$$

then

$$\langle |G'(u, v)|^2 \rangle = |F'(u, v)|^2 \langle |T'(u, v)|^2 \rangle, \tag{7.5-11}$$

where

$$F'(u, v) = F(u, v) * P(u, v)$$

and $\langle |T'(u, v)|^2 \rangle$ is a transfer function that can be measured by observing a point source. The exponential, $p(x, y) = \exp(-2\pi a x)$, has the required property. From the data we have thus extracted the power spectrum of the object, $|F(u, v)|^2$, and that of the exponentially filtered object, $|F'(u, v)|^2$; these together, in principle, contain sufficient information to reconstruct the object intensity.

In practice, in the two-dimensional case, an iterative algorithm similar to that described in Section 7.4 is used to obtain the object intensity $f(x, y)$ from these two power spectra, which are both used alternately as Fourier constraints [59]. Figure 7.5-4 shows an example of reconstructions obtained in a computer simulation with this algorithm.

6. Phase Averaging Method

The instantaneous image intensity $g(x, y)$ is related to the object intensity $f(x, y)$ by the usual convolution formula, which in Fourier space becomes a product:

$$G(u, v) = F(u, v)T(u, v), \tag{7.5-12}$$

where $T(u, v)$ is the instantaneous transfer function of the atmosphere/telescope combination. Taking the ensemble average of the logarithm of Eq. (7.5-12) and equating imaginary parts, we obtain

$$\langle \text{phase}\{G(u, v)\} \rangle = \text{phase}\{F(u, v)\} + \langle \text{phase}\{T(u, v)\} \rangle + 2\pi q, \tag{7.5-13}$$

where the phase is the unwrapped value in the interval $-\infty$ to $+\infty$ and q is an integer. McGlamery [60] suggested that if $\langle \text{phase}\{T(u, v)\} \rangle$ is known (or zero), then the phase of the object transform could be found from the average phase of the image transform. Using the central limit theorem, it is possible to show that, for spatial frequencies $r_0/\lambda z < (u, v) < (D - r_0)/\lambda z$, the quantity $T(u, v)$ is a circular complex Gaussian process, with the result that $\langle \text{phase}\{T(u, v)\} \rangle = 0$.
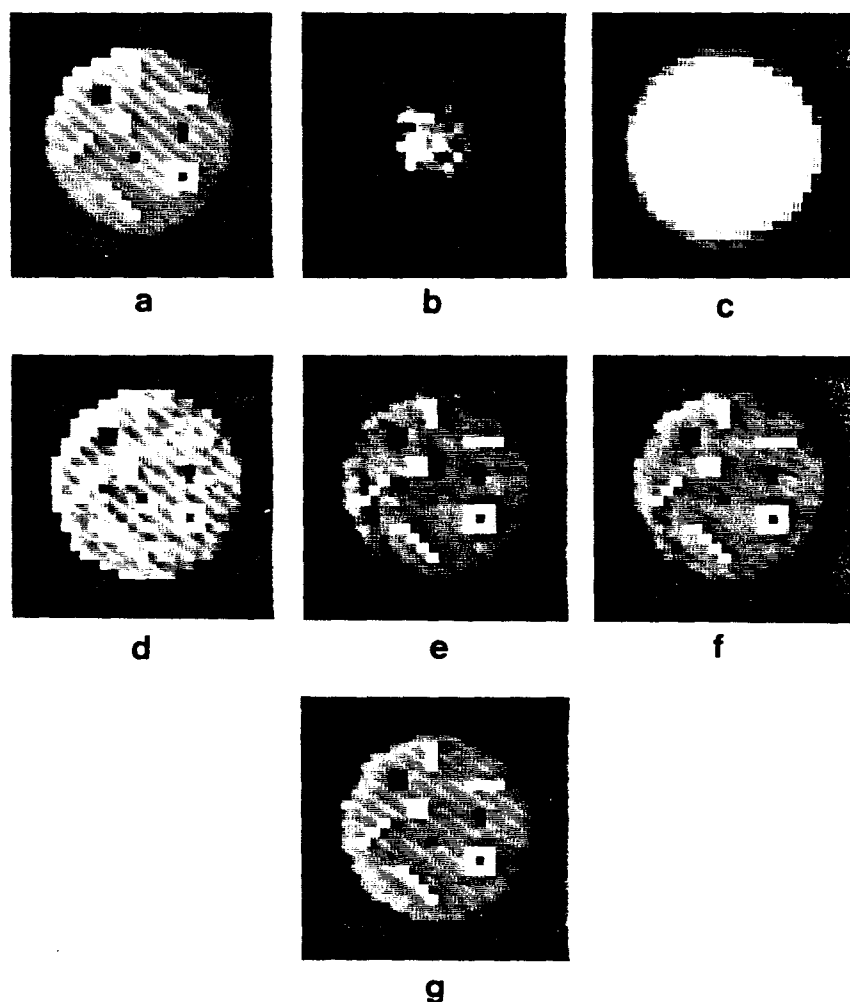
Fig. 7.5-4. Illustration of the exponential filter method. (a) Test object; (b) a short-exposure point spread function; (c) a short-exposure image; (d-g) reconstructions using, respectively, 10, 25, 50, and 100 simulated point and object exposures. (Courtesy of J. W. Walker, Kings College, London.)

The real problem with this phase averaging method is determining, using continuity of $G(u, v)$, the unwrapped phase (the phase in the interval $-\infty$ to $+\infty$) from the phase of $G(u, v)$, which is necessarily in the interval $-\pi$ to $+\pi$. This unwrapping has to be done before the averaging process. When the modulus $|G(u, v)|$ is small, the rms absolute error σ in the unwrapped

phase is given approximately by

$$\sigma \simeq \frac{1}{\sqrt{2}\,\bar{N}\,|G(u,\,v)|},\qquad\qquad (7.5\text{-}14)$$

where $\bar{N}$ is the average number of detected photons per frame and $G(u,\,v)$ is normalized to unity at zero spatial frequency. In addition to having a low *average* value of its modulus [because of the form of the speckle transfer function, Eq. (7.5-2)], the continuous function $G(u,\,v)$, since it is the Fourier transform of a speckle pattern, also contains many points whose modulus is zero, which can be expected to cause problems in phase unwrapping algorithms [61].

Mertz [62] has suggested that it should be possible to use continuity in *time*, as well as spatial frequency, to help unwrap the phase, and such a proposal may be easy to implement using the time-ordered photon event detectors that are becoming available.

7. Non-redundant Aperture Methods

As is well known, the Fourier transform of any intensity point spread function is equal to the autocorrelation of the complex amplitude distribution over the pupil. A given spatial frequency component is therefore the sum (or integral) of products of values of the complex amplitude at all combinations of two points in the pupil separated by a fixed amount. If a special mask of subapertures is used in the pupil, such that no vector separation occurs more than once (i.e., a *nonredundant* array of subapertures), then each spatial frequency component of the point spread function equals the product of two particular values of the complex amplitude in the pupil and hence yields the phase difference between the wave front at these two points. Thus, the Fourier transform of the image intensity, when the imaging aperture is a nonredundant array of subapertures, has a simple, direct interpretation in terms of the wave front in the telescope aperture, and this has been the basis of several possible methods of diffraction-limited imaging from (speckle-free) image plane data. However, in all cases each frame of data has to have an excellent signal-to-noise ratio so that an accurate phase difference can be found.

Three methods of utilizing short-exposure images taken through nonredundant apertures have been put forward. Rhodes and Goodman [63] suggested using two or more masks to form two or more short-exposure images with the same atmospheric distortion—this procedure could be used to eliminate telescope aberrations as well. Brown [64] suggested that even a single image from a single mask could be processed by using a suitable

"sharpness" criterion for the reconstructed object. Finally, there is the possibility of phase averaging analogous to that described in Section 7.5.A.6.

A variation on the use of a nonredundant aperture has been proposed by Greenaway [65]. The basic idea is to reconfigure a redundant aperture into a nearly nonredundant one by using a suitable interferometer and then applying phase closure techniques. This allows the full aperture to be utilized, but it is not clear how one constructs the optical system required to reconfigure the aperture.

8. Phase Diversity Method

As seen in Section 7.5.A.5, the availability of more than one type of measurement opens up additional possibilities for reconstructing an image. A class of such techniques are those that employ phase diversity in the pupil of the telescope [66]. Two images are collected simultaneously: the usual aberrated image with optical transfer function $T(u, v)$ and Fourier transform

$$G(u, v) = F(u, v) T(u, v), \qquad (7.5\text{-}15)$$

and a "phase-diversity" image with optical transfer function $T_d(u, v)$ and Fourier transform

$$G_d(u, v) = F(u, v) T_d(u, v). \qquad (7.5\text{-}16)$$

The phase-diversity transfer function $T_d(u, v)$ includes a known, purposely induced phase aberration in addition to the same unknown atmospherically induced aberrations included in $T(u, v)$. For this problem both the object and the atmospheric aberrations are unknown.

To solve this problem, Gonsalves [66] introduced the error metric

$$E = \int\int [|G(u, v) - \hat{F}(u, v)\hat{T}(u, v)|^2 + |G_d(u, v) - \hat{F}(u, v)\hat{T}_d(u, v)|^2] \, du \, dv$$

$$(7.5\text{-}17)$$

(where $\hat{X}$ is an estimate of X). By the method of calculus of variations, the function $\hat{F}(u, v)$ that minimizes E can be determined and inserted in Eq. (7.5-17) to yield an expression for the error metric that is independent of $\hat{F}(u, v)$:

$$E = \int\int \left[\frac{|G(u, v)\hat{T}_d(u, v) - G_d(u, v)\hat{T}(u, v)|^2}{|\hat{T}(u, v)|^2 + |\hat{T}_d(u, v)|^2} \right] du \, dv. \qquad (7.5\text{-}18)$$

This error metric depends only on the estimates of the transfer functions, which in turn depend only on the estimate of the phase aberrations. One can iteratively search for the estimate of the phase aberrations (usually

parameterized by, say, the coefficients of a Zernike polynomial expansion) that minimize E, by the Fletcher–Powell gradient search method, for example. Having found the aberrations, $T(u, v)$ can be computed and $F(u, v)$ can be determined from Eq. (7.5-15) or, better, by Wiener filtering.

A problem with this method is that, employing only a single pair of frames of data, it works well only for bright objects.

B. Object Recovery from Michelson Interferometry Data

1. Pupil Plane Interferometry

In pupil plane interferometry, the spatial coherence function of starlight is measured by simple two-beam interference either directly in the pupil of a large telescope or with two (or more) separated telescopes in a long-baseline arrangement.

The spatial coherence function $C(\Delta\xi, \Delta\eta)$ is defined by

$$C(\Delta\xi, \Delta\eta) \equiv \langle V(\xi, \eta, t) V^*(\xi + \Delta\xi, \eta + \Delta\eta, t) \rangle, \qquad (7.5\text{-}19)$$

where $V(\xi, \eta, t)$ is the analytic signal representation of the field in the (ξ, η) plane. The real part of $C(\Delta\xi, \Delta\eta)$ can be measured by interfering portions of the wave front located at (ξ, η) and $(\xi + \Delta\xi, \eta + \Delta\eta)$ and measuring the resultant time-average[†] intensity:

$$\langle | V(\xi, \eta, t) + V(\xi + \Delta\xi, \eta + \Delta\eta, t) |^2 \rangle$$
$$= I(\xi, \eta) + I(\xi + \Delta\xi, \eta + \Delta\eta) + 2\,\mathrm{Re}[C(\Delta\xi, \Delta\eta)]. \quad (7.5\text{-}20)$$

The imaginary part is found by retarding one wave front by $\pi/2$ prior to interference. In practice, the two wave fronts are combined either through a beamsplitter arrangement to yield both the real and imaginary parts of $C(\Delta\xi, \Delta\eta)$ simultaneously, or at an angle so that the fringe position gives the phase (if it is possible to follow individual fringes).

According to the van Cittert–Zernike theorem, the coherence function $C(\Delta\xi, \Delta\eta)$ is proportional to the Fourier transform $F(u, v)$ of the object intensity $f(x, y)$; if we take the object coordinates referred to image space, the spatial frequencies (u, v) of the object transform are related to separation in the pupil plane $(\Delta\xi, \Delta\eta)$ given by

$$u = \Delta\xi/\lambda z, \qquad v = \Delta\eta/\lambda z,$$

where z is the focal length of the telescope.[‡]

---

† Or ensemble average; the distinction is unimportant for ergodic light sources such as stars.

‡ It is customary in astronomy to use angular frequencies $\Delta\xi/\lambda$ and $\Delta\eta/\lambda$.

Although historically this method was first proposed and demonstrated by Fizeau and Stephan, it is normally known as Michelson interferometry, following Michelson's measurements of the satellites of Jupiter and the red giant α-Orionis, the latter with a specifically constructed two-beam interferometer mounted on the 100-in. Mt. Wilson telescope. The main attraction of the implementation of Michelson interferometry with two small telescopes is that the baseline, which in terms of resolution is equivalent to the diameter of a single-aperture telescope, can potentially be very large, perhaps 1 km or more. It is also relatively easily adapted to use in space. The major disadvantages of the two-telescope approach are the poor coverage of the (u, v) plane and the lack of reliable phase information.

2. Wave Front Rotational Shearing Method

This method is equivalent to an array of Michelson interferometers working in parallel and is an alternative to speckle (image plane) methods for single large telescopes. Mertz [67] was the first to point out that a rotational shearing interferometer can be used to measure the two-dimensional Fourier transform of any incoherent source distribution with a variable magnification that depends on the amount of rotational shear. This interferometer has been adapted by Roddier and Roddier [68] for astronomical observation.

In a rotational shearing interferometer, the time-varying complex amplitude in the telescope pupil, $V_1(\xi, \eta, t)$, is divided by a beamsplitter into two beams, one of which is rotated by an angle θ with respect to the other before recombination at the same or another beamsplitter. Variable magnification is achieved by varying θ, but to see the principle of operation we shall let $\theta = 180°$. The output intensity $I_2(\xi, \eta)$ of the interferometer in this case is

$$I_2(\xi, \eta) = \langle |V_1(\xi, \eta, t) + V_1(-\xi, -\eta, t)|^2 \rangle$$

$$= 2I_1(\xi, \eta) + 2 \operatorname{Re}[C(2\xi, 2\eta)] \qquad (7.5\text{-}21)$$

for a uniform pupil intensity. The imaginary part of the spatial coherence could be found separately by phase-shifting one beam prior to recombination or, more simply, by adding tilt fringes to form a sideband hologram [68].

In applying this method to imaging through turbulence, it is important to note that the fringe *visibility*, from which the spatial coherence is found, remains constant from frame to frame and the turbulence affects only the detailed form of the fringes. The major disadvantage of the technique is that each frame must have sufficient signal-to-noise ratio to enable the fringe

visibility to be determined, and this requires that the individual fringes are clearly defined. This is a significant drawback despite the fact that at high light levels pupil plane interferometers have a higher signal-to-noise ratio than the image plane technique of speckle interferometry.

3. Phase Closure

Phase retrieval in the two (or more) telescope arrangement originally proposed by Michelson is very much more complicated than for the single-aperture case, as there are almost certainly discontinuities of the measurements in the pupil plane because the full aperture is sparsely filled. One approach is to combine simultaneously the outputs from a nonredundant coherent array and use the image plane (speckle) data as described in Section 7.5.A.7. Another technique, originally suggested and used in radio astronomy [69], is to form simultaneously all possible pair correlations from N apertures by using the Michelson technique to determine the Fourier phase, and then use the principle of *phase closure* to eliminate some or (given enough redundant measurements) all the (unknown) atmospheric phase disturbances.

Consider any three apertures and let the (constant) phases across them due to atmospheric turbulence or other phase errors be α_1, α_2, and α_3. The measurement of instantaneous fringe positions for each aperture pair yields phase differences β_{12}, β_{23}, and β_{13}, which are related to the true object phase differences ψ_{12}, ψ_{23}, and ψ_{13} by

$$\beta_{12} = \psi_{12} + \alpha_1 - \alpha_2,$$

$$\beta_{23} = \psi_{23} + \alpha_2 - \alpha_3,$$

$$\beta_{13} = \psi_{13} + \alpha_1 - \alpha_3.$$

By forming the sum

$$\beta_{12} + \beta_{23} - \beta_{13} = \psi_{12} + \psi_{23} - \psi_{13},$$

the atmospheric phase terms are eliminated. If one assumes that two object phases are known, then the third can be calculated. The arbitrary choice of the first two phases simply affects the position of the reconstructed object on the sky and does not affect its morphology. By repeating this with a carefully chosen set of aperture spacings (which include redundant spacings) it is possible to determine the Fourier phase of the object at all spatial frequencies covered by the array. Even if sufficient redundant spacings are not present to ensure a complete reconstruction, the number of unknown phases is greatly reduced by the phase closure method.

7.6 CONCLUSIONS

The methods for reconstructing stellar objects $f(x, y)$ from interferometric data in optical astronomy fall into two classes: those that require only the Fourier modulus $|F(u, v)|$ and those that use the additional, but limited, phase data that are available in certain observational techniques.

It appears that object reconstruction from the Fourier modulus alone is usually unique, although it is not difficult to construct specific counter-examples that do not yield a unique solution. The main problem is how to find this solution. The iterative transform algorithm described in Section 7.4 is the most computationally efficient and successful algorithm to date. Using array processors of modest cost, a complete iteration on a 128×128 data set need take only about 1 s and convergence to a solution can be obtained in a few minutes if stagnation problems are avoided (see Section 7.4.C).

Particular observing techniques, such as speckle interferometry, can provide not only the Fourier modulus but also Fourier phase information. Clearly, if this additional information is available, it should be used in the reconstruction process. The most promising techniques for doing this at the moment are the cross-spectrum, triple correlation, and exponential filter methods described in Sections 7.5.A.3-5 respectively.

The planned construction of several giant 10-20-m diameter ground-based optical telescopes in the near future should provide the stimulation for further advances in phase retrieval and object reconstruction in astronomy.

ACKNOWLEDGMENTS

REFERENCES

1. J. W. Goodman (1984). "Statistical Optics," Wiley, New York.
2. R. H. T. Bates (1982). *Astronomical speckle imaging. Physics Reports (Reviews Sect. of Phys. Lett.)* **90**, 203-297.
3. J. C. Dainty (1984). "Laser Speckle and Related Phenomena," Springer Verlag, Heidelberg. 2nd edition, pp. 255-320.
4. J. C. Dainty (1984). Progress in image reconstruction in astronomy. *Proc. SPIE*, **492**.
5. A. Walther (1963). The question of phase retrieval in optics. *Optica Acta* **10**, 41-49.
6. A. H. Greenaway (1977). Proposal for phase recovery from a single intensity distribution. *Opt. Lett.* **1**, 10-12.
7. T. R. Crimmins and J. R. Fienup (1981). Ambiguity of phase retrieval for functions with disconnected support. *J. Opt. Soc. Am.* **71**, 1026-1028.

8. T. R. Crimmins and J. R. Fienup (1983). Uniqueness of phase retrieval for functions with sufficiently disconnected support. *J. Opt. Soc. Am.* **73**, 218-221.

9. J. R. Fienup (1978). Reconstruction of an object from the modulus of its Fourier transform. *Opt. Lett.* **3**, 27-29.

10. P. J. Napier and R. H. T. Bates (1974). Inferring phase information from modulus information in two-dimensional aperture synthesis. *Astron. Astrophys. Suppl.* **15**, 427-430.

11. W. Lawton (1980). A numerical algorithm for 2-D wavefront reconstruction from intensity measurements in a single plane. *Proc. SPIE* **231**, 94-98.

12. M. Nieto-Vesperinas (1980). Dispersion relations in two dimensions: Application to the phase problem. *Optik (Stuttgart)* **56**, 377-384.

13. I. Manolitsakis (1982). Two-dimensional scattered fields: A description in terms of the zeros of entire functions. *J. Math. Physics* **23**, 2291-2298.

14. R. Barakat and G. Newsam (1984). Necessary conditions for a unique solution to two-dimensional phase recovery. *J. Math. Phys.* **25**, 3190-3193.

15. J. L. C. Sanz and T. S. Huang (1983). Unique reconstruction of a band-limited multi-dimensional signal from its phase or magnitude. *J. Opt. Soc. Am.* **73**, 1446-1450.

16. Yu. M. Bruck and L. G. Sodin (1979). On the ambiguity of the image reconstruction problem. *Opt. Commun.* **30**, 304-308.

17. M. A. Fiddy, B. J. Brames, and J. C. Dainty (1983). Enforcing irreducibility for phase retrieval in two dimensions. *Opt. Lett.* **8**, 96-98.

18. J. R. Fienup (1983). Reconstruction of objects having latent reference points. *J. Opt. Soc. Am.* **73**, 1421-1426.

19. B. J. Brames (1985). Uniqueness and other aspects of the optical phase problem. Ph.D. Thesis, University of Rochester.

20. T. R. Crimmins (1986). Phase retrieval for discrete functions with support constraints: summary, *in* OSA Topical Meeting on Signal Recovery and Synthesis II, Honolulu, Hawaii.

21. J. L. C. Sanz, T. S. Huang, and F. Cukierman (1983). Stability of unique Fourier-transform phase reconstruction. *J. Opt. Soc. Am.* **73**, 1142-1145.

22. E. N. Leith and J. Upatnieks (1962). Reconstructed wavefronts and communication theory. *J. Opt. Soc. Am.* **52**, 1123-1130.

23. J. W. Goodman (1970). Analogy between holography and interferometric image formation. *J. Opt. Soc. Am.* **60**, 506-509.

24. C. Y. C. Liu and A. W. Lohmann (1973). High resolution image formation through the turbulent atmosphere. *Opt. Commun.* **8**, 372-377.

25. J. R. Fienup, T. R. Crimmins, and W. Holsztynski (1982). Reconstruction of the support of an object from the support of its autocorrelation. *J. Opt. Soc. Am.* **72**, 610-624.

26. G. H. Stout and L. H. Jensen (1968). "X-ray Structure Determination," Macmillan, London.

27. J. E. Baldwin and P. J. Warner (1978). Phaseless aperture synthesis. *Mon. Not. R. Astr. Soc.* **182**, 411-422.

28. B. R. Frieden and D. G. Currie (1976). On unfolding the autocorrelation function. *J. Opt. Soc. Am.* **66**, 1111A.

29. J. R. Fienup (1982). Phase retrieval algorithms: A comparison. *Appl. Opt.* **21**, 2758-2769.

30. H. V. Deighton, M. S. Scivier, and M. A. Fiddy (1985). Solution of the two-dimensional phase retrieval problem. *Opt. Lett.* **10**, 250-251.

31. H. H. Arsenault and S. Lowenthal (1969). La restitution de la phase a de measures d'eclairement. *C.R. Acad. Sc. Paris* **269**, 518-521.

32. H. H. Arsenault and K. Chalasinska-Macukow (1983). The solution to the phase retrieval problem using the sampling theorem. *Opt. Commun.* **47**, 380-386.

33. K. Chalasinska-Macukow and H. H. Arsenault (1985). Fast iterative solution to exact equations for the two-dimensional phase-retrieval problem. *J. Opt. Soc. Am. A* **2**, 46-50.

34. R. H. T. Bates, et al. (1982). Fourier phase problems are uniquely solvable in more than one dimension. I: underlying theory. *Optik* **61**, 247-262; (1982) II: one-dimensional considerations. *Optik* **62**, 131-142; (1982) III: computational examples for two dimensions. *Optik* **62**, 219-230.

35. R. W. Gerchberg and W. O. Saxton (1972). A practical algorithm for the determination of phase from image and diffraction plane pictures. *Optik* **35**, 237-246.

36. R. W. Gerchberg (1974). Super-resolution through error energy reduction. *Optica Acta* **21**, 709-720.

37. W. O. Saxton (1978). "Computer Techniques for Image Processing in Electron Microscopy," Academic Press, New York.

38. J. R. Fienup (1979). Space object imaging through the turbulent atmosphere. *Opt. Eng.* **18**, 529-534.

39. J. R. Fienup (1981). Reconstruction and synthesis applications of an iterative algorithm. *Proc. SPIE* **373**, 147-160.

40. J. R. Fienup (1984). Phase retrieval from a single intensity distribution, in "Optics in Modern Science and Technology," Conference Digest for ICO-13, August 20-24, Sapporo, Japan, pp. 606-609; J. R. Fienup (1987). Reconstruction of a complex-valued object from the modulus of its Fourier transform using a support constraint. *J. Opt. Soc. Am. A* **3** (forthcoming).

41. J. R. Fienup and G. B. Feldkamp (1980). Astronomical imaging by processing stellar speckle interferometry data. *Proc. SPIE* **243**, 95-102.

42. R. J. Sault (1983). The Fourier phase problem, *FLEURS Internal Report No. 83/1*, University of Sydney.

43. P van Toorn, A. H. Greenaway, and A. M. J. Huiser (1984). Phaseless object reconstruction. *Optica Acta* **7**, 767-774.

44. J. R. Fienup (1984). Experimental evidence of the uniqueness of phase retrieval from intensity data. *In* "Indirect Imaging," Proceedings of URSI/IAU Symposium, Sydney, Australia, (J. A. Roberts, ed.), pp. 99-109, Cambridge University Press, Cambridge.

45. J. R. Fienup and C. C. Wackerman (1986). Phase retrieval stagnation problems and solutions. *J. Opt. Soc. Am. A* **2** (forthcoming).

46. G. B. Feldkamp and J. R. Fienup (1980). Noise properties of images reconstructed from Fourier modulus. *Proc. SPIE* **231**, 84-93.

47. A. Labeyrie (1970). Attainment of diffraction limited resolution in large telescopes by Fourier analysing speckle patterns in star images. *Astron. and Astrophys.* **6**, 85-87.

48. J. W. Goodman and J. F. Belsher (1976). Fundamental limitations in linearly invariant restoration of atmospherically degraded images. *Proc SPIE* **75**, 141-154.

49. C. R. Lynds, S. P. Worden, and J. W. Harvey (1976). Digital image reconstruction applied to Alpha Orionis. *Astrophys. J.* **207**, 174-180.

50. R. H. T. Bates and F. M. Cady (1980). Towards true imaging by wideband speckle interferometry. *Opt. Commun.* **32**, 365-369.

51. B. R. Hunt, W. R. Fright, and R. H. T. Bates (1983). Analysis of the shift-and-add method for imaging through turbulent media. *J. Opt. Soc. Am.* **73**, 456.

52. K. T. Knox and B. J. Thompson (1974). Recovery of images from atmospherically degraded short-exposure photographs. *Astrophys. J. Letters* **193**, L45-L48.

53. M. Rimmer (1974). Method for evaluating lateral shearing interferograms. *Appl. Opt.* **13**, 623-629.

54. B. R. Hunt (1979). Matrix formulation of the reconstruction of phase values from phase differences. *J. Opt. Soc. Am.* **69**, 393-399.

55. A. W. Lohmann, G. Weigelt, and B. Wirnitzer (1983). Speckle masking in astronomy: triple correlation theory and applications. *Appl. Opt.* **22**, 4028-4037.

56. H. Bartelt, A. W. Lohmann, and B. Wirnitzer (1984). Phase and amplitude recovery from bispectra. *Appl. Opt.* 23, 3121-3129.

57. B. J. Brames and J. C. Dainty (1981). Method for determining object intensity distributions in stellar speckle interferometry. *J. Opt. Soc. Am.* 71, 1542-1545.

58. J. G. Walker (1981). The phase retrieval problem: A solution based on zero location by exponential apodization. *Optica Acta* 28, 735-738.

59. J. G. Walker (1982). Computer simulation of a method for object reconstruction from stellar speckle interferometry data. *Appl. Opt.* 21, 3132-3137.

60. B. L. McGlamery (1970). Image restoration techniques applied to astronomical photography. *In* "Astronomical Use of Television-Type Image Sensors" (V. R. Boscarino, ed.), pp. 167-192, NASA SP-256(NTIS N71-28522).

61. M. S. Scivier, T. J. Hall, and M. A. Fiddy (1984). Phase unwrapping using the complex zeros of a bandlimited function and the presence of ambiguities in two dimensions. *Opt. Acta* 31, 619-623.

62. L. Mertz (1984). Phase estimation with a few photons. *Appl. Opt.* 23, 1638-1641.

63. W. T. Rhodes and J. W. Goodman (1973). Interferometric technique for recording and restoring images degraded by unknown aberrations. *J. Opt. Soc. Am.* 63, 647-657.

64. T. M. Brown (1978). Reconstruction of turbulence degraded images using nonredundant aperture arrays. *J. Opt. Soc. Am.* 68, 883-889.

65. A. H. Greenaway (1982). Diffraction-limited pictures from single turbulence degraded images in astronomy. *Opt. Commun.* 42, 157-161.

66. R. A. Gonsalves (1982). Phase retrieval and diversity in adaptive optics. *Opt. Eng.* 21, 829-832.

67. L. Mertz (1965). "Transformations in Optics," Wiley, New York.

68. C. Roddier and F. Roddier (1979). *In* "Image Formation from Coherence Functions in Astronomy," pp. 175-185. D. Reidel, Amsterdam.

69. R. C. Jennison (1958). A phase sensitive interferometer technique for the measurement of the Fourier transforms of spatial brightness distributions of small angular extent. *Mon. Not. R. Astr. Soc.* 118, 276-284.